

The Warming of the California Current System: Dynamics and Ecosystem Implications

EMANUELE DI LORENZO AND ARTHUR J. MILLER

Scripps Institution of Oceanography, University of California, San Diego, La Jolla, California

NIKLAS SCHNEIDER

International Pacific Research Center, University of Hawaii at Manoa, Honolulu, Hawaii

JAMES C. MCWILLIAMS

Institute of Geophysics and Planetary Physics, University of California, Los Angeles, Los Angeles, California

(Manuscript received 23 March 2003, in final form 24 August 2004)

ABSTRACT

Long-term changes in the observed temperature and salinity along the southern California coast are studied using a four-dimensional space–time analysis of the 52-yr (1949–2000) California Cooperative Oceanic Fisheries Investigations (CalCOFI) hydrography combined with a sensitivity analysis of an eddy-permitting primitive equation ocean model under various forcing scenarios. An overall warming trend of 1.3°C in the ocean surface, a deepening in the depth of the mean thermocline (18 m), and increased stratification between 1950 and 1999 are found to be primarily forced by large-scale decadal fluctuations in surface heat fluxes combined with horizontal advection by the mean currents. After 1998 the surface heat fluxes suggest the beginning of a period of cooling, consistent with colder observed ocean temperatures. Salinity changes are decoupled from temperature and appear to be controlled locally in the coastal ocean by horizontal advection by anomalous currents. A cooling trend of -0.5°C in SST is driven in the ocean model by the 50-yr NCEP wind reanalysis, which contains a positive trend in upwelling-favorable winds along the southern California coast. A net warming trend of $+1^{\circ}\text{C}$ in SST occurs, however, when the effects of observed surface heat fluxes are included as forcing functions in the model. Within 50–100 km of the coast, the ocean model simulations show that increased stratification/deepening of the thermocline associated with the warming reduces the efficiency of coastal upwelling in advecting subsurface waters to the ocean surface, counteracting any effects of the increased strength of the upwelling winds. Such a reduction in upwelling efficiency leads in the model to a freshening of surface coastal waters. Because salinity and nutrients at the coast have similar distributions this must reflect a reduction of the nutrient supply at the coast, which is manifestly important in explaining the observed decline in zooplankton concentration. The increased winds also drive an intensification of the mean currents of the southern California Current System (SCCS). Model mesoscale eddy variance significantly increases in recent decades in response to both the stronger upwelling winds and the warmer upper-ocean temperatures, suggesting that the stability properties of the SCCS have also changed.

1. Introduction

A warming trend of roughly 1°C in sea surface temperature (SST) from 1950 to 1999 has been observed along the southern California coast (Bograd and Lynn 2003; Roemmich 1992). Deepening of the mean thermocline, increasing stratification, and declining zooplankton have been linked with this warming trend (McGowan et al. 2003; Roemmich and McGowan

1995). Studies of large-scale ocean variability have suggested that these SST changes are part of a large-scale Pacific Ocean decadal mode of variability (Chao et al. 2000; Lluch-Cota et al. 2001; Mantua et al. 1997; Zhang et al. 1997). In this mode SST is coherent and in phase along the entire United States and Canadian west coast. However the cause of the warming and its links with ocean dynamics are still obscure.

How are these long-term ocean temperature variations driven in the southern California Current System (SCCS)? Are they a local dynamical response to changes in winds? Are they a simple thermal response to changes in local surface heat fluxes? Are remote forcings important in driving these variations? What is

Corresponding author address: Emanuele Di Lorenzo, School of Earth and Atmospheric Sciences, Georgia Institute of Technology, Atlanta, GA 30332-0340.
E-mail: edl@eas.gatech.edu

the connection with basin-scale variability? How does this thermocline deepening and increased stratification affect the dynamics of the upwelling system, the distribution of nutrients in the euphotic zone, and the oceanic ecosystem?

Previous analyses of observed surface heat fluxes (Cayan 1992) and ocean model hindcasts of the surface layer heat budget over the entire North Pacific Ocean (Miller et al. 1994) suggest that along the California coast the long-term SST signal is dominated by changes in surface heat fluxes. However, it is still unclear whether these findings are consistent with observations in the SCCS. The coastal portion of the warming trend between 1950 and 1999 could also be a result of a decrease in the strength of upwelling winds, which cannot be resolved by the coarse-resolution model used in Miller et al. (1994). Although appealing, this hypothesis is not consistent with the evidence that coastal alongshore winds have increased in recent decades, which would be expected to cool, not warm, SST (Schwing and Mendelssohn 1997, hereinafter SM97). An increase in upwelling-favorable winds is consistent with the ideas of Bakun (1990) and recent regional climate modeling experiments (Snyder et al. 2003), which suggest that alongshore winds intensify as a response to warmer ocean temperatures.

Long-term changes in salinity in the SCCS, which have not been thoroughly investigated, are also important because they represent an independent signature of ocean dynamical response. Are decadal temperature and salinity variations correlated in the SCCS? Can they be explained by similar dynamical mechanisms?

The goal of this paper is to address the preceding questions by studying the available observations together with targeted ocean model experiments. The 52-yr-long California Cooperative Oceanic Fisheries Investigations (CalCOFI) time series of salinity and temperature provides a unique dataset to address these questions. We investigate the processes controlling long-term changes in temperature and salinity in the SCCS by computing a four-dimensional space–time analysis of the 1949–2000 CalCOFI hydrography and executing a sensitivity analysis of a primitive equation ocean model of the California coast driven by various forcings. Although the CalCOFI observations are limited to the Southern California Bight (SCB), the large-scale coherence in the forcing functions and oceanic SST response suggests that the results will be applicable to the entire CCS.

In summary our results suggest that the temperature changes are forced by large-scale surface heat flux variations over the northeast Pacific combined with horizontal advection of anomalies by the mean currents in the SCCS. We demonstrate that the observed thermocline deepening and increased stratification from 1950 to 1999, associated with upper-ocean temperature warming, reduces the efficiency of the upwelling, despite the increase in upwelling favorable winds. The

increased alongshore winds are also found to intensify the mean California Current and mesoscale eddy variability in the model, suggesting changes in the stability properties of the SCCS.

Throughout the paper we will use the phrase “warming trend” to indicate the overall transition toward warmer temperature from 1950 to 1999. This transition has also been called a regime shift, occurring in 1976–77, in previous literature. For the purpose of this study the definition of trend over the period of the data follows from linearly fitting a line to the time series and taking the difference in values at the end points. Over the 52-yr period of CalCOFI data we cannot distinguish a significant trend in SST that might be associated with global warming.

In section 2 we introduce the observational data and the analysis process. We then give a brief description of the primitive equation ocean model and the experimental setup in section 3 and the forcing functions in section 4. In section 5 we present the observed temperature (T) and salinity (S) variability. In section 6 we explain the intensification of the mean currents. In section 7 we discuss the low-frequency salinity variations. In section 8 we explain the temperature variations and the consequent warming trend using simple and full-physics models. In section 9 we identify the effects of warming on changes in coastal upwelling and their impact on nutrient flux to the surface layer. In section 10 we present evidence for an increase in mesoscale eddy variance in recent decades. Section 11 provides a summary of the results.

2. CalCOFI hydrography analysis

From 1949 to the present CalCOFI (available online at <http://www.calcofi.org>) has sampled the upper 500 m of the California coastal ocean. The data consist of in situ measurements of temperature and salinity and also of biological quantities such as chlorophyll- a , nitrate, and zooplankton. The sampling grid in the early cruises extends northward from Baja California up to the coast of Oregon with almost monthly resolution. Starting in 1965, the grid size was reduced to cover only the southern California coast and the temporal resolution became seasonal, although each season is not always sampled during the same month of the year. This introduces temporal aliasing of the seasonal circulation patterns. The data also have gaps during the 1970s and 1980s when few cruises occurred.

Because of the spatial and temporal inhomogeneity of the CalCOFI hydrography, we regrouped the data from all cruises following their temporal and spatial location rather than their cruise number. The resulting data were then rebinned into time snapshots and the date of the snapshot was assigned to be the average time of all data that occur in that bin. This procedure was not done automatically because it is difficult to

identify a unique criterion that will ensure a correct binning. After the binning we retained only the bins that have both temperature and salinity data within the range of values acceptable for this oceanic region. We then gridded each set of binned data with an objective map (Bretherton et al. 1976) for each depth. The along-shore (cross shore) decorrelation length scale used in the mapping is 110 km (100 km) as determined by Chereskin and Trunnell (1996). Of the gridded data we retained only the portion for which the value of the normalized error was below 0.4. To simplify the analysis and the plotting of the data, we also interpolated in time (monthly) the various spatial maps with a temporal objective analysis using a decorrelation time scale of 4 months. This time scale was chosen because on average there are always two maps within any four months period, except during the 1970s and 1980s, which therefore result in gaps.

When reconstructing the low-frequency signals (periods above 3 yr), the error associated with the time interpolation between data gaps was estimated to be 6%–11% of the signal standard deviation (see the appendix). After taking into account the errors from the spatial and temporal mapping, the resulting data used for the analysis in the next sections cover the region between 30° and 34°N with a cross-shore extent of 550 km from the coast (Fig. 1). In the following sections all anomalies (observations and model output) are com-

puted by removing the climatological monthly means. This analysis of the CalCOFI hydrography is now available online at <http://horizon.ucsd.edu/calcofi>.

3. Model experiment setup

a. Primitive equation (PE) ocean model

The ocean model is a regional eddy-resolving primitive equation ocean model called the Regional Ocean Modeling System (ROMS), a descendent of SCRUM (Song and Haidvogel 1994). This model uses a generalized sigma-coordinate system in the vertical direction and a curvilinear grid in the horizontal plane (with average resolution of 9 km). The grid extends roughly 1200 km along the U.S. West Coast from northern Baja to north of San Francisco Bay with approximately 1000 km offshore extent normal to the coast (Fig. 1). The vertical grid has 20 levels with enhanced resolution in the surface and bottom boundary layer (a stretching factor of 5 was used for the surface and 0.4 for the bottom boundary). The model bathymetry is obtained by a smooth interpolation of the ETOPO5 analysis (NGDC 1998) and is characterized by an extended (about 150–200 km) continental shelf in the Southern California Bight (typical depth of 400 m) followed by a steep continental slope offshore (typical depth of 4000 m). The model bathymetry was smoothed in order to

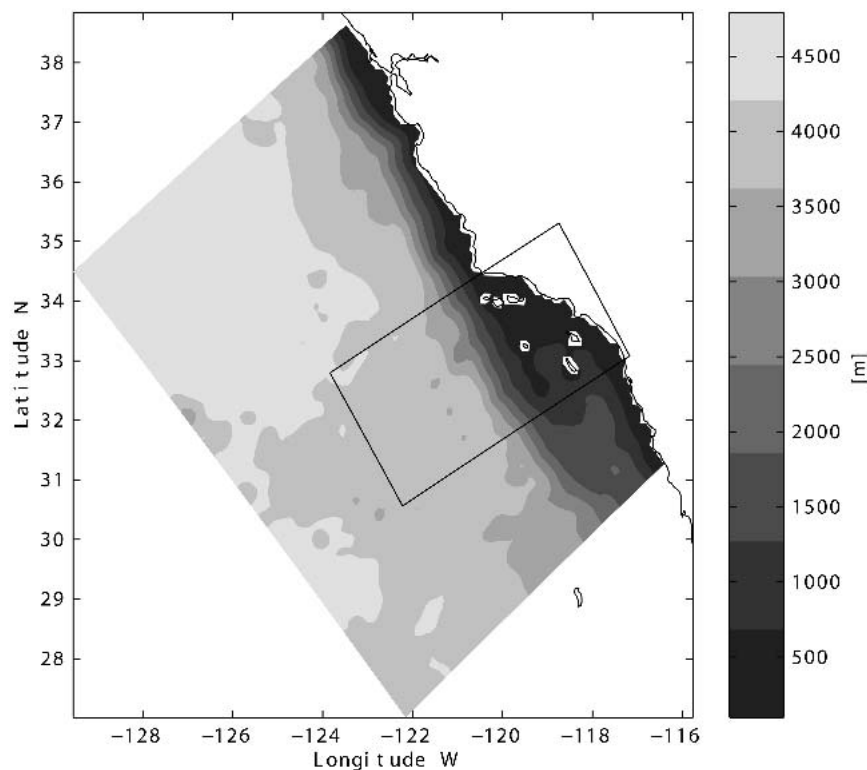


FIG. 1. Model bathymetry for the Southern California Current System. Black rectangle identifies the domain of the CalCOFI data analysis.

keep the topographic slope below 0.2 (also referred as the r factor). A high r factor would lead to errors in the computation of the model pressure gradient (Mellor et al. 1994). In the horizontal plane we do not use explicit diffusivity and rely on implicit diffusivity associated with the third-order upstream biased advection scheme that is used (Shchepetkin and McWilliams 1998). In the vertical direction the mixed layer dynamics are parameterized using a K -profile parameterization (KPP) scheme (Large et al. 1994) and a vertical viscosity and diffusivity coefficient of $10^{-3} \text{ m}^2 \text{ s}^{-1}$. A more complete report of the model numerics is given by Shchepetkin and McWilliams (2005; also Shchepetkin 2003).

A modified radiation condition (Marchesiello et al. 2001), which allows for stable, long-term integration of the model, is used at the three open boundaries together with a nudging term for relaxation to prescribed boundary values. The nudging is stronger (time scale of 1 day) if the direction of the flow is inward and weaker (time scale of 1 yr) if the flow is outward. Using this model configuration, Di Lorenzo (2003) was able to model the dynamics of the seasonal cycle in the SCCS as inferred from CalCOFI observations and assess the sensitivity of the circulation to different wind stress forcing. Marchesiello et al. (2003) have also successfully used this same model to study the long-term equilibrium structure of the California Current over the entire U.S. West Coast.

b. Experiment configurations

The sensitivity experiments for the various forcing functions are summarized in Table 1. Each row represents a separate 51-yr integration starting in January 1950 and ending in December 2000. We performed four model experiments labeled A–D in column 1. The types of forcing functions used for the sensitivity analysis are mechanical surface forcing by the wind stress, buoyancy forcing associated with surface heat fluxes, and open boundary nudging of temperature and salinity (indicated in the remaining columns in Table 1). The labels of the forcing functions are as follows.

1) CLIMA

A 12-month climatology is used to force repetitively each year of a model simulation from 1950 to 2000. The climatologies for the different surface forcings are derived by taking averages of the time-dependent forcing

functions, which are described next. For temperature and salinity climatologies we use Levitus et al. (1994) and Levitus and Boyer (1994).

2) NCEP

The 51-yr monthly averaged winds from the National Centers for Environmental Prediction (NCEP; Kalnay et al. 1996) from 1950 to 2000 are used as mechanical forcing.

3) CALCOFI

The long-term temperature changes at the model open boundaries are represented by adding a constant value at each vertical level, for each month. This value is defined as the difference between the observed and climatological mean values averaged over the CalCOFI box (Fig. 1). This imposes the observed time-dependent changes of vertical stratification at the open boundaries of the model but does not change the horizontal gradients. This approach is consistent with observations that low frequency temperature anomalies are coherent, in phase, and of the same amplitude over the entire U.S. West Coast. (Lluch-Cota et al. 2001; Mantua et al. 1997; Zhang et al. 1997). Because we do not introduce any horizontal gradients, the strength of the horizontal advection at the open boundaries remains unchanged enabling us to assess the role of the mean advection of temperature anomalies in the temperature budget.

4) COADS

Net surface heat fluxes at monthly temporal resolution and 1° spatial resolution from 1950 to 2000 from an updated Cayan (1992) analysis of the Comprehensive Ocean–Atmosphere Data Set (COADS) are used as thermal forcing.

To maintain consistency in the comparison of model and observations, the model output has been subsampled spatially and temporally at the same resolution as CalCOFI and then objectively mapped. The model analysis was also compared with the one obtained by retaining the full model field and no significant differences were found in the low-frequency signals with periods above 3 yr. The full model fields are retained in the discussion on changes in eddy variability, which cannot be resolved from the current observational sampling.

4. Model surface forcings

a. Net surface heat fluxes

A spatial characterization of the net surface heat flux $Q(x,y,t)$ over the eastern North Pacific is given by the first empirical orthogonal function (EOF) that explains 58% of the variance (Fig. 2a). This mode is coherent and in phase over a much larger area than the CalCOFI data domain. The time series of the amplitude associated with this first EOF [referred to as the principal

TABLE 1. Primitive equation model experiments. Columns 2–5 list the type of forcing data used in the experiments (see text for details).

Expt	Wind stress	Heat flux	OBC	
			temperature	salinity
A	CLIMA	CLIMA	CLIMA	CLIMA
B	NCEP	CLIMA	CLIMA	CLIMA
C	NCEP	COADS	CLIMA	CLIMA
D	NCEP	COADS	CALCOFI	CLIMA

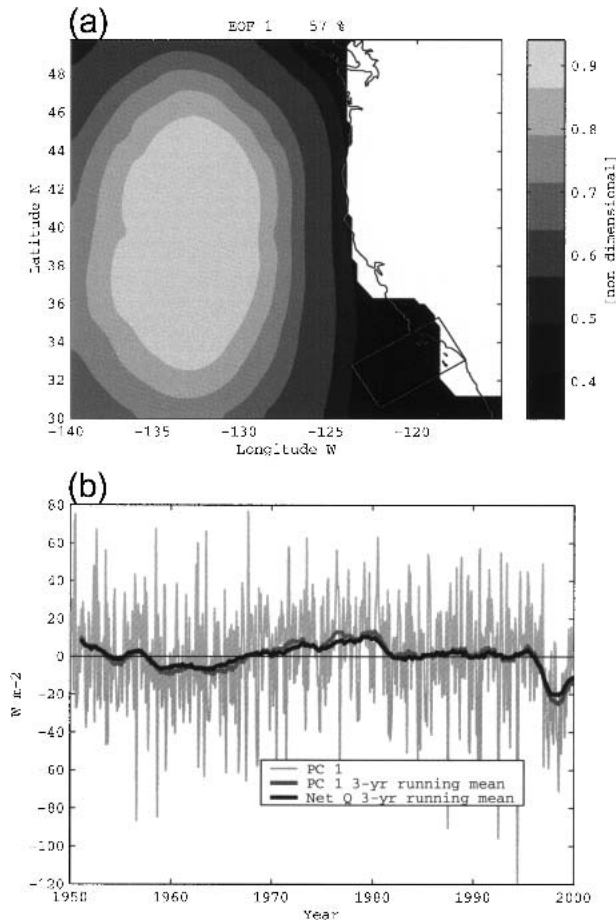


FIG. 2. (a) EOF 1 for the net surface heat flux anomaly (seasonal cycle removed) from D. Cayan (2003, personal communication). The black box identifies the location of the CalCOFI data domain. (b) PC 1 (light gray lines) and domain average net heat flux anomaly. The 3-yr running mean for PC 1 is correlated 0.9 with the correspondent domain average net heat flux anomaly (black thick line).

component (PC)] is strongly correlated ($r = 0.9$) to the time series of heat flux anomalies averaged over the smaller CalCOFI data domain (Fig. 2b). This time series shows a period of negative fluxes during the 1960s followed by a period of positive fluxes into the ocean in the 1970s. The 1980s and early 1990s do not have significant anomalies. The end of the 1990s marks the beginning of a period of negative fluxes.

b. NCEP wind stress

A spatial and temporal characterization of the 51-yr NCEP wind stress reanalysis within the PE model domain is given by the first EOF of alongshore winds and wind stress curl anomalies for the upwelling season (April–July) from 1950 to 2000 (Fig. 3). The first mode for the alongshore wind stress anomaly (explaining 72% of the variance) is uniformly negative (upwelling favorable) with a region of stronger amplitude near the

coast north of the Southern California Bight. The corresponding PC for this mode (Fig. 4a) reveals strong interannual variability and a trend toward increased upwelling-favorable winds. The first EOF for wind stress curl anomaly shows a pattern that is similar to the mean wind stress curl in this region with positive curl in the SCB and negative offshore (Bakun and Nelson 1991; Winant and Dorman 1997). The temporal evolution of this mode (not shown) is well correlated with that of the alongshore wind stress anomalies (Fig. 4a).

A trend in upwelling favorable winds along the California coast was also identified by Bakun (1990) and SM97 (Fig. 4b) through analyses of raw COADS and coastal station observations. A comparison between the NCEP and SM97 equatorward winds in the SCCS reveals a remarkable correspondence after 1962 at interannual to decadal time scales (Figs. 4b,c). Before 1962 the SM97 winds are more upwelling favorable than NCEP so that the trend is stronger in NCEP winds (0.019 N m^{-2} over this period, which is equivalent to a 10% change with respect to the mean alongshore wind stresses in this region). This discrepancy will yield an uncertainty in ocean model estimates of the long-term changes in upwelling over the last 50 years. However, the sign of the response is not in doubt since both wind datasets exhibit a clear positive trend.

5. Observed temperature, salinity, and velocity changes

To provide a dynamical framework to understand the long-term changes in the oceanic conditions of the SCCS, we will first describe the observed mean circulation patterns averaged from 1949 to 2000. We will then proceed to characterize the spatial and temporal variability of T , S , and alongshore geostrophic currents.

a. The mean circulation from 1949 to 2000

At the surface the circulation (Fig. 5a) is characterized by broad equatorward flow [California Current (CC)] in the offshore region, poleward flow close to the coast [Inshore Countercurrent (IC)], and a region of cyclonic circulation [Southern California Eddy (SCE)] that connects the inshore and the offshore circulation (Chereskin and Trunell 1996; Di Lorenzo 2003; Lynn and Simpson 1987). At depth, below the mixed layer, the core of the CC is still well defined and the signature of the SCE is stronger (Fig. 5b). The coastal poleward flow that closes the recirculation region of the SCE is referred to as the California Undercurrent (CU) in the literature. This current brings warm salty water from the south into the SCB. In contrast the offshore water masses of northern origin are cold and fresh.

b. Observed temperature and salinity variability

We now describe the observed anomalies for T , S , and depth of the 26.4 isopycnal ($Z_{26.4}$). The anomalies

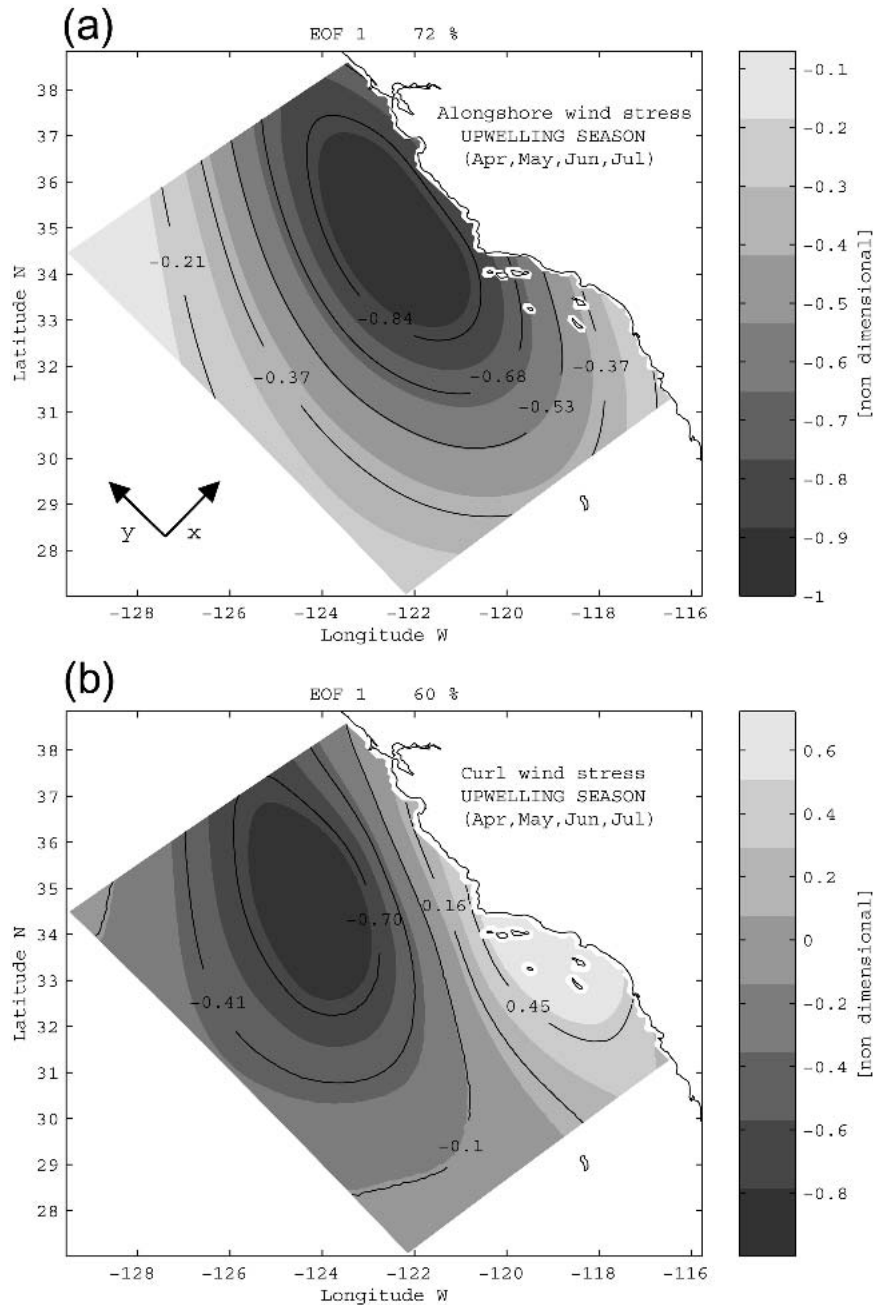


FIG. 3. (a) EOF mode 1 for alongshore wind stress anomalies (seasonal cycle removed) during the upwelling season. Alongshore is defined along the y axis of the model grid. (b) EOF 1 for wind stress curl anomalies. The data are extracted from the NCEP reanalysis and interpolated over the PE model domain.

are computed by removing the climatological monthly means. The depth of the 26.4 isopycnal ranges seasonally between 180 and 220 m and is always located below the surface mixed layer.

The time series of anomalies for surface T and S , and depth of the 26.4 isopycnal ($Z_{26.4}$), averaged over the southern California CalCOFI domain (Fig. 6a,b), display prominent low-frequency variability (periods

above 3 yr). Temperature is dominated by interannual variability and is well correlated with indices of large-scale climate variability such as ENSO and the Pacific decadal oscillation (PDO) (Mantua et al. 1997). In contrast, salinity is dominated by interdecadal variability and is not coherent with large-scale climate indices (Schneider et al. 2005, hereinafter SDN). The T and S signals appear to be uncorrelated on time scales longer

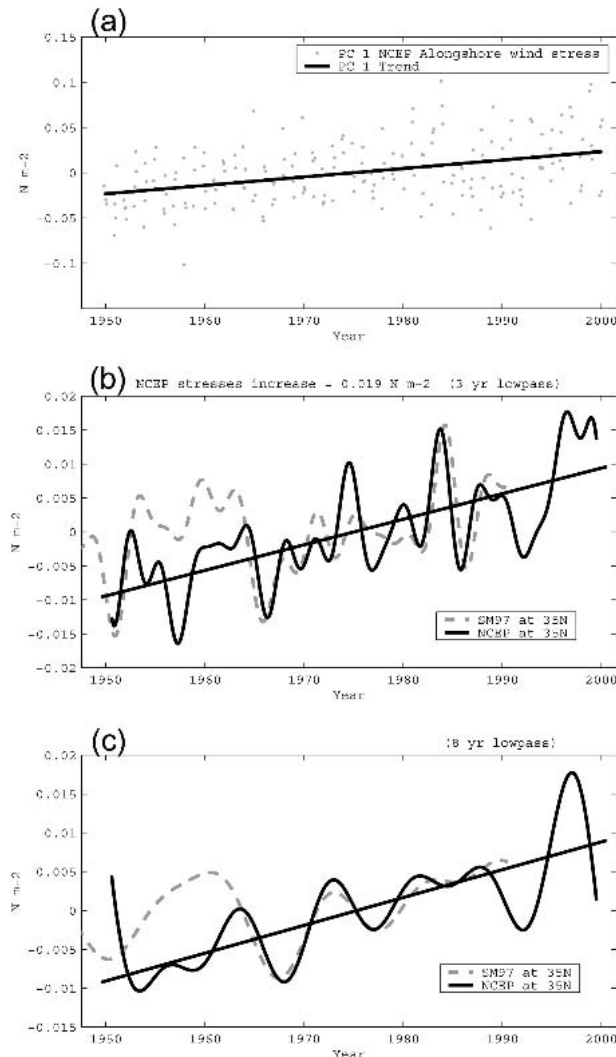


FIG. 4. Plot of (a) PC 1 for alongshore wind stress anomalies (Apr, May, Jun, Jul) in Fig. 3a. (b) Alongshore wind stress monthly anomalies (seasonal cycle removed) for NCEP (black) and Schwing and Mendelsohn (1997) COADS analysis (gray). A 3-yr low-pass filter is applied. (c) Same data as (b) but with an 8-yr low-pass filter applied. The increase in wind stress is computed as the difference between year 2000 and 1950 from a linear fit to the NCEP time series.

than a few years. The temperature signal exhibits a warming trend of 1.3°C over the last 52 years. An 18-m deepening of $Z_{26.4}$ is correlated with this warming. The salinity signal exhibits a weak negative trend over the length of the record (-0.03 psu). Such a trend is not significant when compared with the standard deviation of the salinity signal. However recent studies of long-term changes in the SCCS (Bograd and Lynn 2003) have attributed some significance to this freshening in the nearshore where the trend is stronger and the low-frequency modulation weaker.

The spatial structure of T and S variability is summarized by EOF 1 of the signals averaged from the

surface to the $Z_{26.4}$. It shows that the low-frequency variations seen in the time series are associated with like-signed structures spanning the entire data domain (Fig. 7). The first salinity EOF is characterized by a core of higher variance located around the offshore branch of the SCE in correspondence with the mean location of the CC. The first temperature EOF has a weak inshore–offshore gradient but smaller spatial scales than the salinity EOF mode.

To characterize the vertical structure of these low-frequency changes we also compute vertical EOFs along an averaged transect, W1 in Fig. 5. PC 1 of temperature captures the warming trend (Figs. 8a and 8b). It extends to 200 m and varies weakly in the cross-shore direction. The temporal dependence of this mode is very well correlated with the temperature time series in Fig. 6a. The first vertical salinity EOF (Fig. 8c) shows that the offshore core of maximum variance (400 km from the coast, centered at longitude -121.5°W), previously identified in the horizontal EOFs, is found to extend to 200 m. At the coast the signal is shallower and weaker.

Vertical sections for the difference in means for T and S (Fig. 9) over the period E1 (1950–70) and E2 (1980–2000) show a warming (Fig. 9f) of roughly 1°C and an isopycnal deepening of roughly 20 m. The core of the warming is located offshore, coincident with a core of low-salinity water (roughly -0.05 psu). The low-salinity waters are also found inshore in the surface layers (Fig. 9e). A core of saltier water (roughly 0.05 psu) is evident closer to shore at depth. The same analysis performed on other sections showed similar results.

c. Alongshore geostrophic current variability

The transect W1 intersects the center of the mean location of the SCE (Fig. 5b). At this location the signature of the SCE is very strong and less affected by the noise in the data that come from the aliasing of mesoscale eddies, which are poorly resolved by CalCOFI. To characterize the variability in intensity of the SCE we perform a vertical EOF of the alongshore total geostrophic flow (including the mean) computed from the CalCOFI temperature and salinity (Fig. 8e) relative to 500 m. In the computation of geostrophic velocities, T and S were extrapolated by means of objective mapping in areas shallower than 500 m. The topography is shown in each vertical section and there are only a few points shallower than 500 m. Vertical EOF 1 shows alongshore velocity with equatorward flow offshore and poleward flow inshore. The temporal evolution of this pattern (Fig. 8f) contains a strong mean component (the SCE) along with a positive trend from the late 1950s to the present, suggesting an intensification of the recirculation region of the SCE. The total variance explained by this mode is 60% and the amount of variance associated with the trend component alone is 30%. The higher modes contain no evidence of a trend

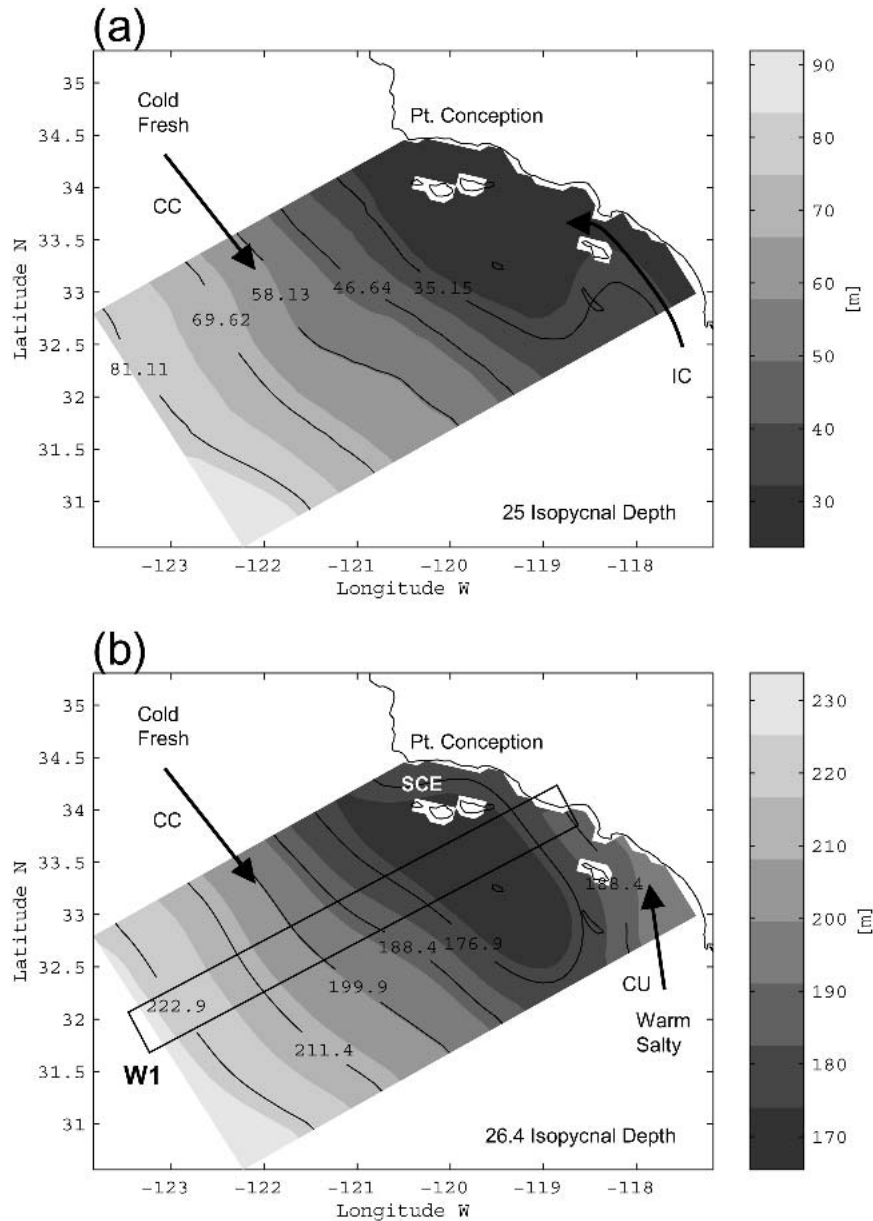


FIG. 5. Average depths of isopycnal (a) 25 and (b) 26.4 from CalCOFI observation for the period 1949–2000 as an indication for surface and deeper flow field.

and capture the displacement of the CC core on inter-annual time scales.

In the following section we discuss and interpret the dynamics that contribute to each of the observed signals using the output of the circulation model. We start with the currents and then consider salinity and temperature.

6. Intensification of ocean currents

In the previous section we found observational evidence of an intensification of the recirculation region of

the SCE over the last 50 years. Model studies of the SCCS show that the SCE linearly responds to changes in amplitude of the mean wind stress curl (Di Lorenzo 2003). A Hovmoeller plot of the 51-yr NCEP wind stress curl anomalies in the CalCOFI domain (Fig. 10a) shows a period of more negative curl in the coastal region before 1980, and then a transition to stronger positive curl after 1980. To investigate and isolate the changes in ocean circulation associated with these changes in the winds we force the ocean model with the 50-yr time-dependent NCEP wind forcing and climatological condition for all other forcing functions (expt B

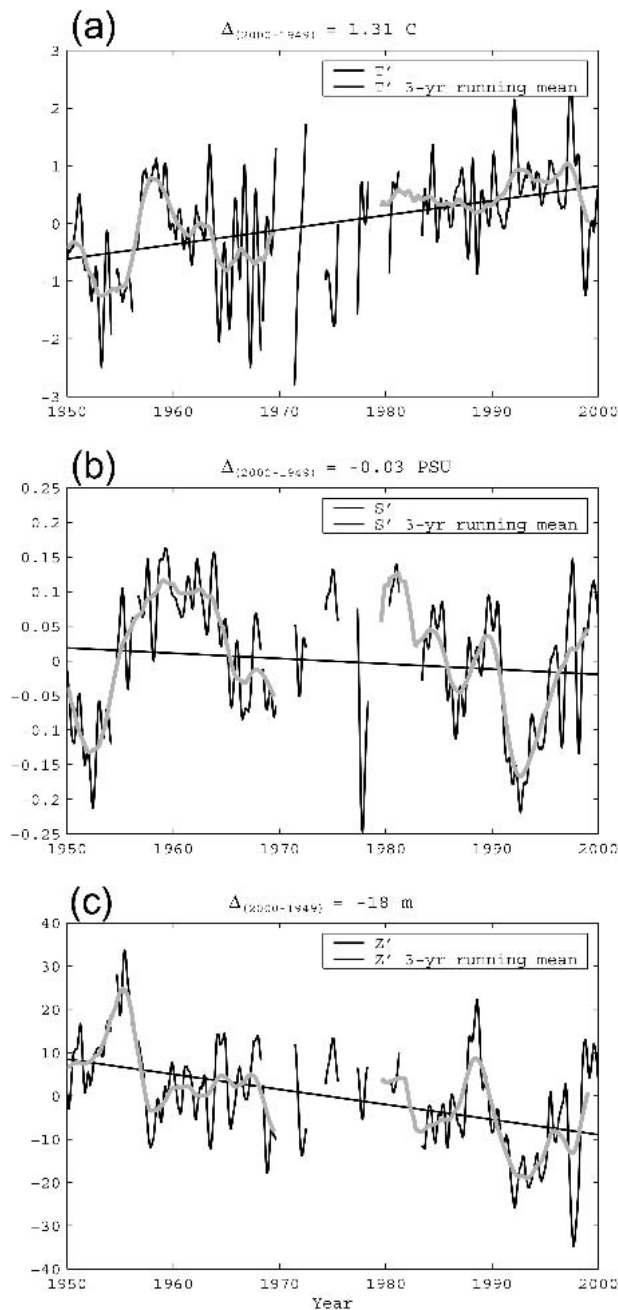


FIG. 6. Time series of observed (a) surface temperature and (b) salinity anomalies averaged over the CalCOFI data domain. (c) Time series of the isopycnal 26.4-depth anomaly. The seasonal cycle is removed in all the time series.

in Table 1). The model response shows anomalously high (low) free-surface elevation during the period before (after) 1980 (Fig. 10b). This is particularly evident near the coast. After 1980 the cross-shore gradient in free surface height becomes stronger, indicating an intensification of the southward surface currents.

A comparison of vertical sections (Fig. 11) of geostrophic flow computed from CalCOFI and model be-

fore and after 1980 show that the model intensification of the SCE is consistent with the observations. The observations, however, show a stronger intensification of the SCE between the two periods with differences in magnitudes of roughly $2\text{--}3\text{ cm s}^{-1}$. The spatial structure of this response is also evident in the first EOF mode of the model free-surface elevation (Fig. 12a). This shows that after 1980 the alongshore velocity is more southward in the offshore branch of the recirculation region and more northward inshore.

In the model, the offshore equatorward flow (the CC) intensifies as a response to the trend in the winds. The model also exhibits strong interannual variability in the cross-shore velocities as evident from the cross-shore variability of the CC's core (Fig. 10b). Model sensitivity experiments (not shown) reveal that such variability can be induced by cross-shore variations of the zero wind stress curl line and by changes in the eddy strength. Because of the low spatial variability in the NCEP wind stress curl (due to the coarse resolution of NCEP), we attribute most of the model cross-shore variability to changes in the eddy field. Such changes are part of the intrinsic variability of the CCS and are not necessarily a directly forced response.

7. Low-frequency salinity variations

a. The offshore region

The low-frequency salinity variations (Fig. 6b) do not correlate with any index of large-scale climate variability, such as the PDO and ENSO (SDN), suggesting that local dynamics in the CCS are important in explaining the salinity budget. The vertical EOF 1 of salinity (Fig. 8c) shows that the low-frequency signal is centered offshore in the location of the mean core of the CCS. This suggests that meandering and changes in the strength of the CCS underlie these low-frequency salinity variations. Indeed, SDN show that these oscillations are consistent with a model of anomalous advection, wherein the net effect of changes in advection generates a low-frequency salinity signal.

A comparison of the time evolution of model average surface salinity (expt B) with the CalCOFI observations (Fig. 13a) shows that, while the model hindcast captures the correct amplitude of the interannual salinity signal, the phase of the two signals do not agree. Adding the warming trend to the model forcing functions does not significantly improve the correlation (Fig. 13b).

Assuming that the observed low-frequency salinity variability is attributable to anomalous advection, the model's poor performance can be explained by one or all of the following hypotheses: 1) the largest fraction of the variability of the California Current is intrinsic, in which case the model would not be able to capture the true realization of the 50 years of data; 2) the spatial and temporal resolutions of the local forcing functions are not sufficient to capture the deterministic

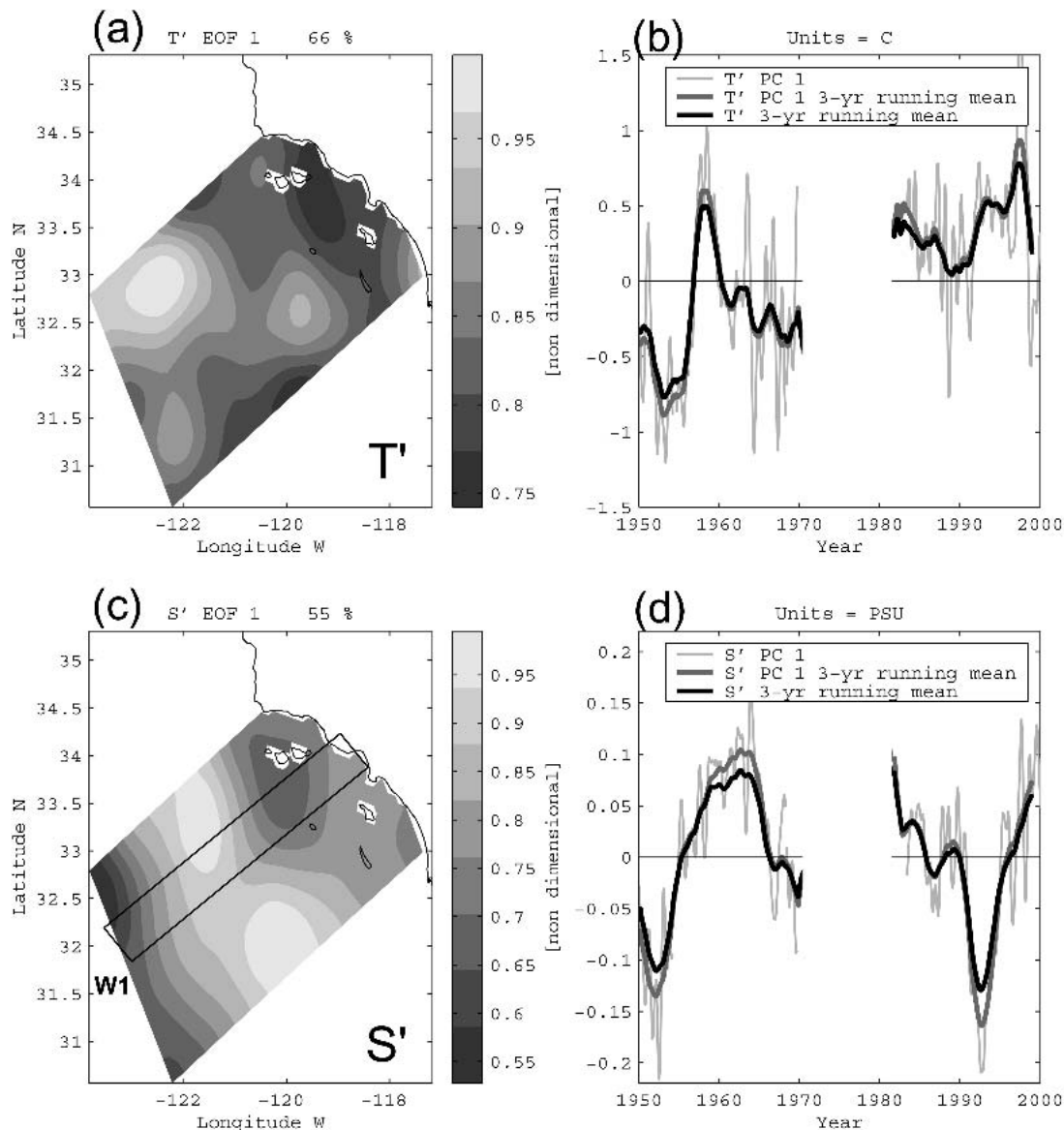


FIG. 7. EOF1 for depth average (a) temperature and (c) salinity anomalies from the CalCOFI data analysis and their respective (b),(d) PC 1. The volume average temperature and salinity time series are superimposed on the PC 1 in (b) and (d). The seasonal cycle is removed before performing the analysis. The depth average extends from the surface to the 26.4 isopycnal in all computations.

component of the anomalous advection; and/or 3) the remote oceanic forcing through coastally trapped waves, which are missing in the model simulations, represent an important contribution to the variability of the currents.

Based on several modeling studies, we argue that intrinsic variability may play a central role in low frequency salinity variations. Using a model forced by climatological winds and heat fluxes, Marchesiello et al. (2003) show that most of the variance in the currents is intrinsic to the CCS. Di Lorenzo (2003) confirms this finding by comparing linearized and nonlinear versions

of the ROMS model for the CCS, both forced with climatological forcing. In this study, the nonlinear component of the circulation associated with synoptic mesoscale eddies is able to generate low-frequency variance. More targeted numerical simulations are needed to assess the relative contributions of the various processes and forcings.

b. The nearshore region

The anomalous advection model used to explain low-frequency variations in the offshore region does not

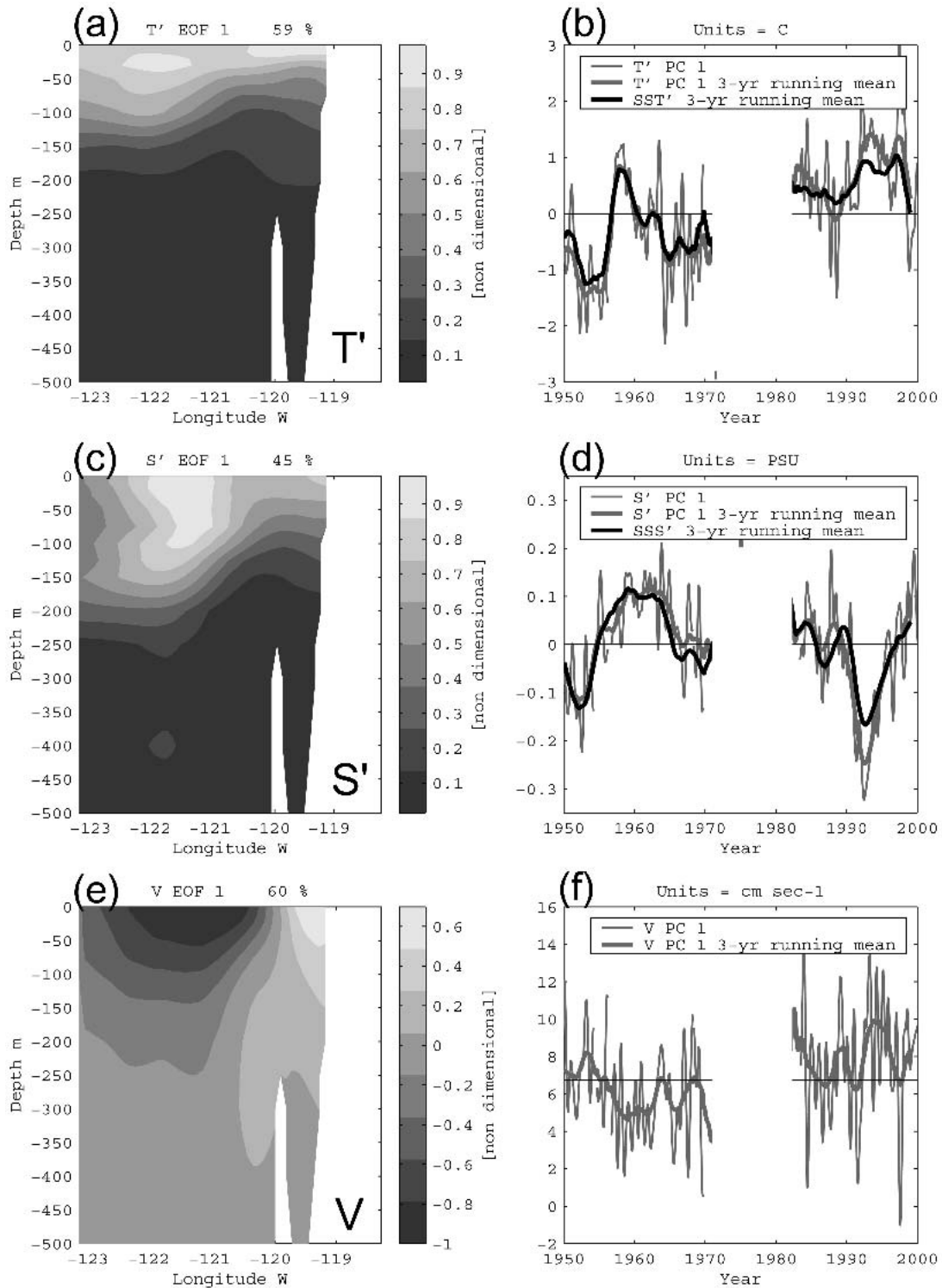


FIG. 8. Vertical EOFs 1 on transect W1 (Fig. 5) for the CalCOFI (a),(b) temperature and (c),(d) salinity anomalies. The seasonal cycle is removed. (e),(f) EOF 1 for geostrophic alongshore currents relative to 500 m. This transect was found to be representative for various cross sections in the CalCOFI domain.

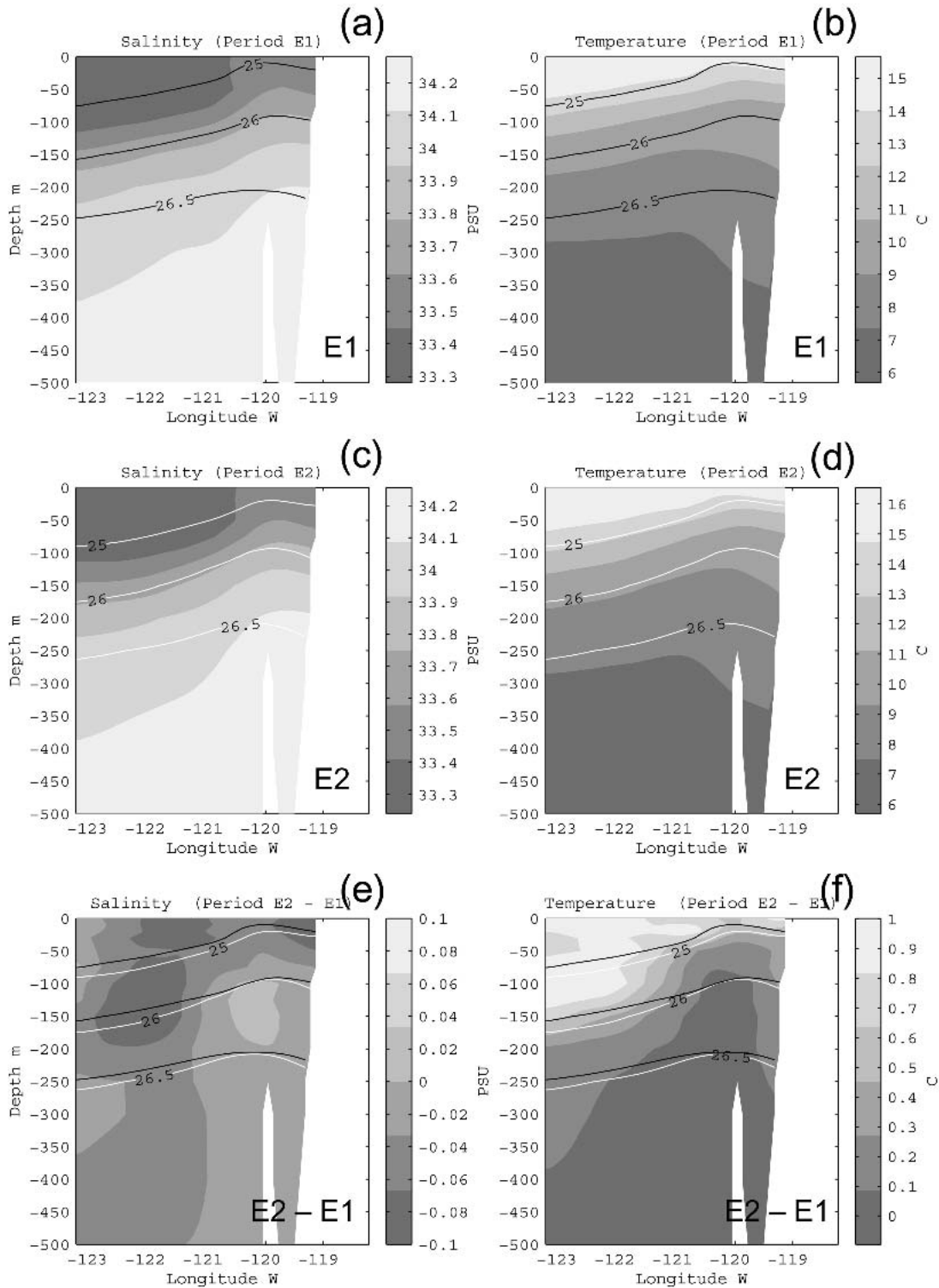


FIG. 9. Vertical sections of mean (a),(c),(d) salinity and (b),(d),(f) temperature along transect W1. Label E1 denotes the mean for 1950–70, E2 is the mean for 1980–2000, and E2 – E1 is their difference. This transect was found to be representative for various cross sections in the CalCOFI domain. Isopycnal depths for the periods E1 (black) and E2 (white) are superimposed to show the deepening of the isopycnals for 1980–2000.

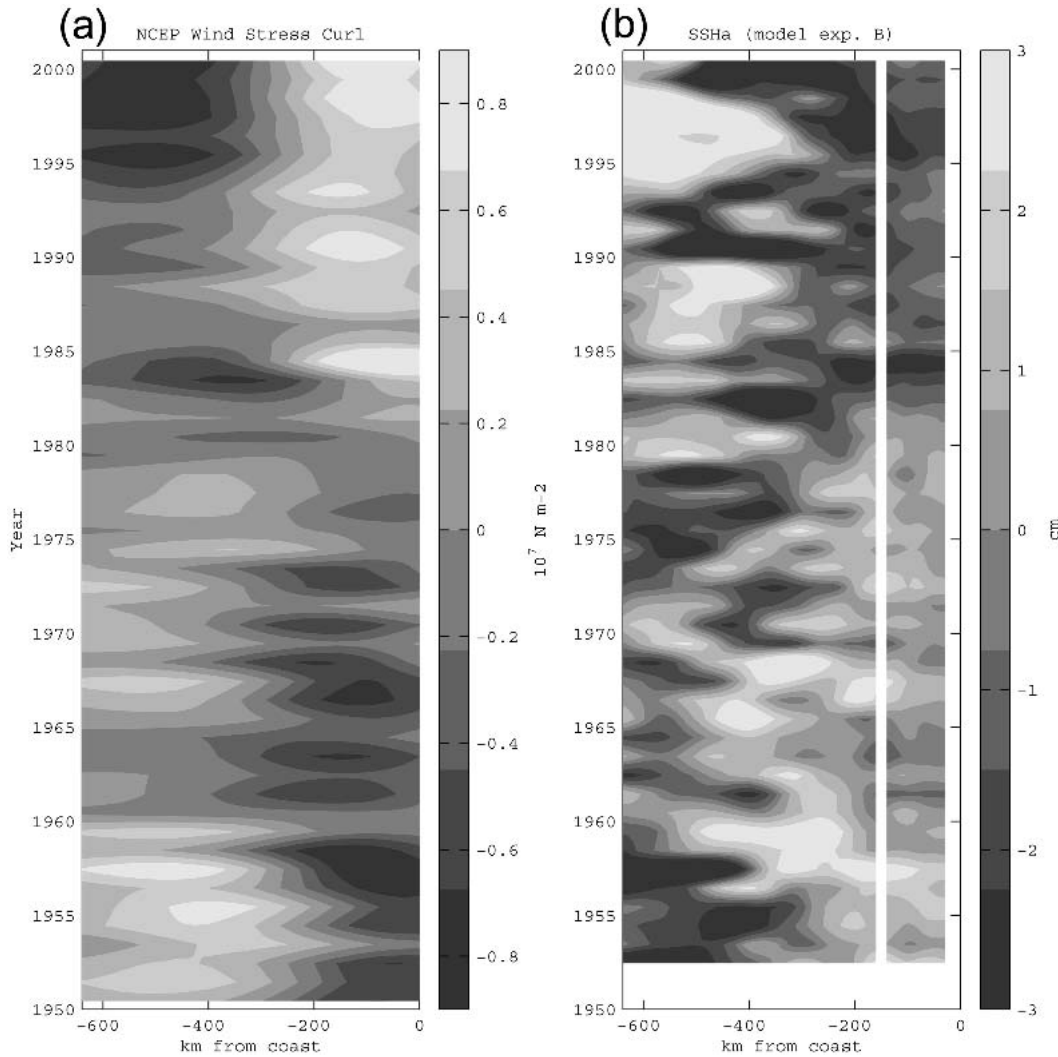


FIG. 10. (a) Hovmoeller diagram for NCEP wind stress curl anomaly and the response of (b) model SSH. The anomalies are computed by removing the seasonal cycle. This experiment shows the strong forced response of the circulation to changes in the winds. The x direction is cross-shore distance from the coast. This transect was found to be representative for various cross sections in the CalCOFI domain.

apply to salinity variations near the coast. In fact, surface salinity measurements from the Scripps Pier are not significantly correlated with the low-frequency fluctuations observed in the CalCOFI average. Instead, coastal salinity variability is best described as a freshening trend over the period 1950–2000 (McGowan et al. 2003; Bograd and Lynn 2003). Di Lorenzo (2003, Fig. 9) shows that external forcing functions linearly control the dynamics of the coastal region, in contrast with the offshore region which is dominated by nonlinear processes.

Following this idea, we attempt to isolate the linear response of the model's salinity to external forcing (i.e., the winds and warming trend) by computing the first EOFs for experiments B and D (Figs. 12c and 12e). These EOFs explain a small fraction of the variance

and show a similar pattern characterized by a tongue of high variance in the location of the CC's core. The temporal evolution of this mode (PC 1; Figs. 12d and 12f) is characterized by interdecadal variations and a negative trend. This trend is associated with an overall freshening in the location of the CC's core, which can be ascribed to the increased southward transport of fresher water masses (SSHa; Figs. 12a and 12b) that result from upwelling favorable winds. Conversely, in the near shore, the increased coastal upwelling brings saltier subsurface water into the coastal surface layer [note that EOF 1 changes sign near the coast in expt B (Fig. 12c)]. However, when the effects of the warming trend are included in the model (expt D; Fig. 12e), the resulting increase in the stratification of the water column inhibits the ability

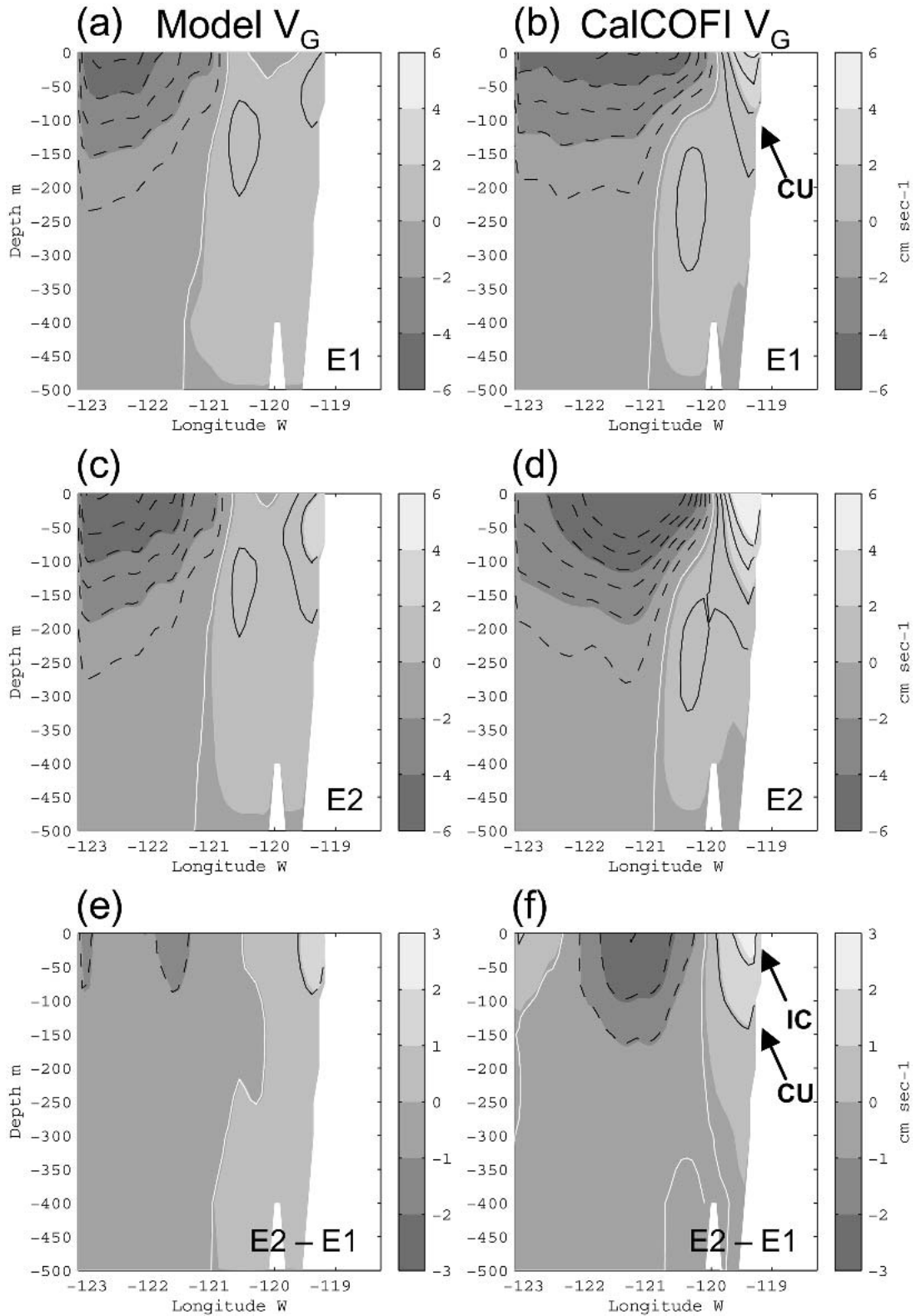


FIG. 11. Vertical sections for (a),(c),(e) alongshore model and (b),(d),(f) CalCOFI geostrophic velocity along transect W1. Label E1 is the mean for 1950–70, E2 is the mean for 1980–2000, and E2 – E1 is their difference. This transect is representative for various cross sections in the CalCOFI domain. The geostrophic calculation for both model and observation assumes a level of no motion at 500 m.

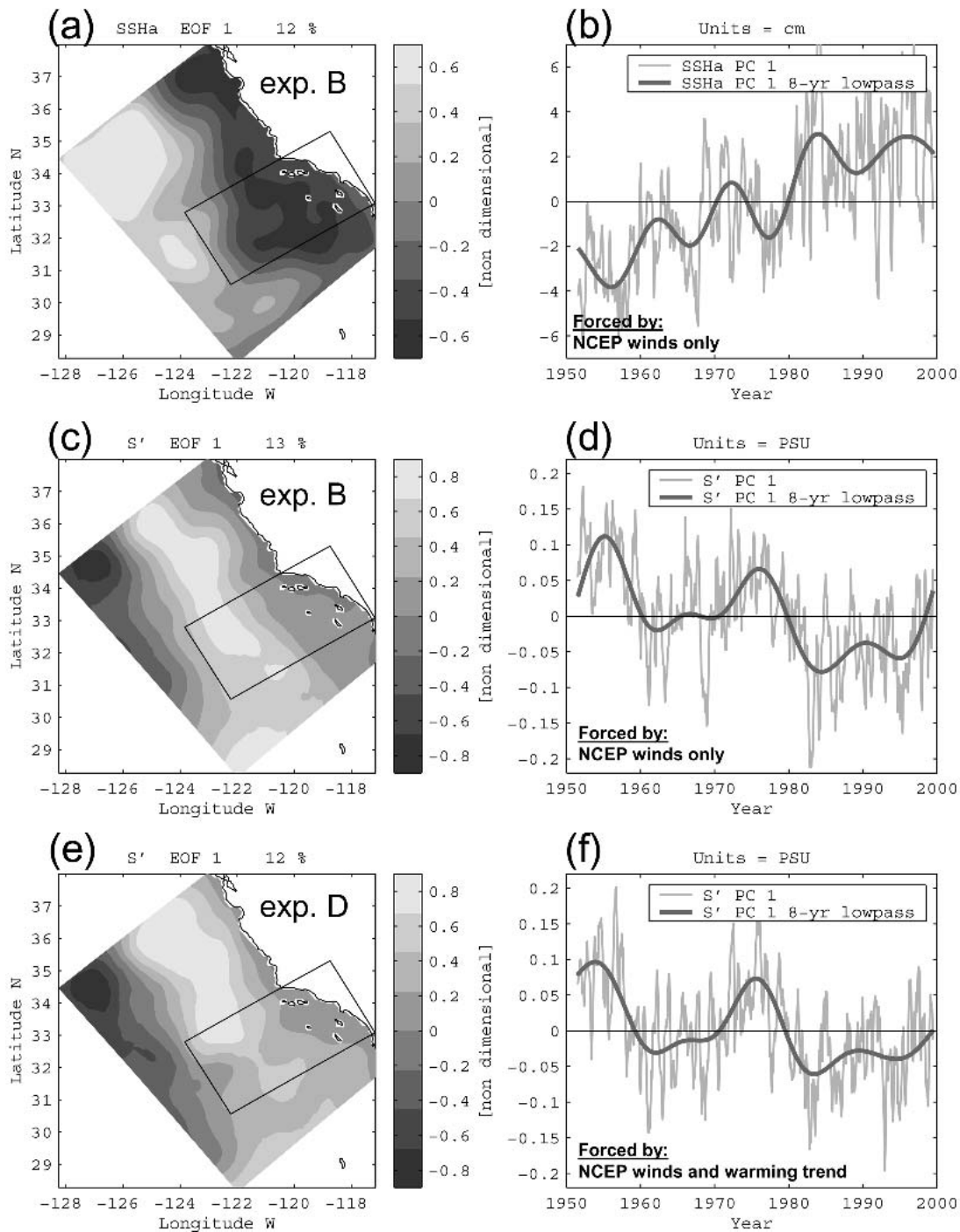


FIG. 12. Model EOF 1 for (a),(b) SSH and (c),(d) surface salinity anomalies for expt B forced by NCEP winds only. Model EOF 1 for (e),(f) surface salinity anomalies for expt D forced with NCEP winds and the warming trend. The seasonal cycle was removed.

of upwelling to supply saltier subsurface water to the surface (in this case, the EOF does not change sign). This leads to a freshening along the coast, in agreement with observations. The effect of increased stratification is strong enough to counteract the effect of

the wind-induced trend toward saltier coastal waters. A more detailed discussion of the relationship between coastal salinity, upwelling, and nutrient availability is presented in the section on changes in upwelling.

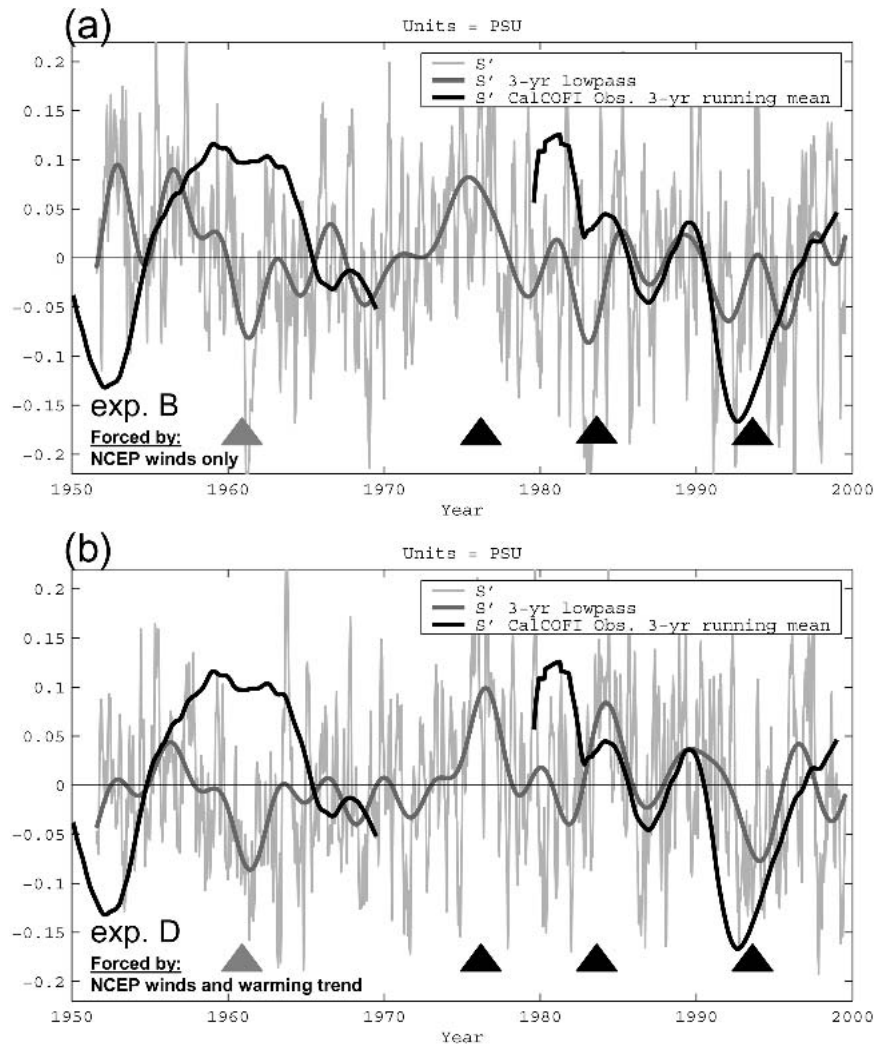


FIG. 13. Model surface salinity averaged in the CalCOFI box. (a) Experiment forced only by the time-dependent NCEP winds. (b) Experiment forced by the time-dependent NCEP winds and warming trend. These time series do not capture the observed salinity signal in CalCOFI [(b), black line] but have comparable amplitude. The 3-yr low-pass model time series in (a) and (b) are also not well correlated. The correlation coefficient is $r = 0.4$. The 95% significance level is $r = 0.5$ and for 99% is $r = 0.62$. The black (gray) triangles mark some of the larger peaks in expt D time series that are different (similar) from expt B. In expt D, the addition of surface heat fluxes and stratification through the temperature open boundary condition is sufficient to change the low-frequency salinity signal.

8. Temperature warming trend

The spatial and temporal variability of CalCOFI upper-ocean temperature is correlated with the PDO. This mode of large-scale SST variability is characterized by coherent and in-phase changes of SST along the entire U.S. and Canadian west coasts. Although this indicates that temperature changes in the SCCS are part of a large-scale response, it is still unclear if this response is driven locally by changes in large-scale forcing functions, such as surface winds and heat fluxes, or remotely by large-scale changes in ocean advection,

which modulate the input of cold water masses from the north.

In the previous section we noted that changes in advection have been proposed to explain the modulation of the salinity signal. The fact that temperature and salinity variability are uncorrelated over long time scales (periods above 3 yr) suggests that changes in oceanic advection are not the dominant mechanism controlling temperature changes over the last 50 years and that the upper-ocean temperature may be primarily controlled by the surface forcing functions. These forcing functions are the winds and the heat fluxes. In this

section we will discuss the potential role of each of these forcings.

a. Local response to wind stresses

We start by considering the PE model response to local changes in the NCEP surface winds (expt B).

These winds contain a positive trend in northwesterly winds that tends to increase the upwelling of cold water masses. The model response to these winds (in isolation) is captured by EOF 1 of model SST (Figs. 14a,b) explaining 29% of the variance. This mode shows a clear cooling trend with colder waters inshore and

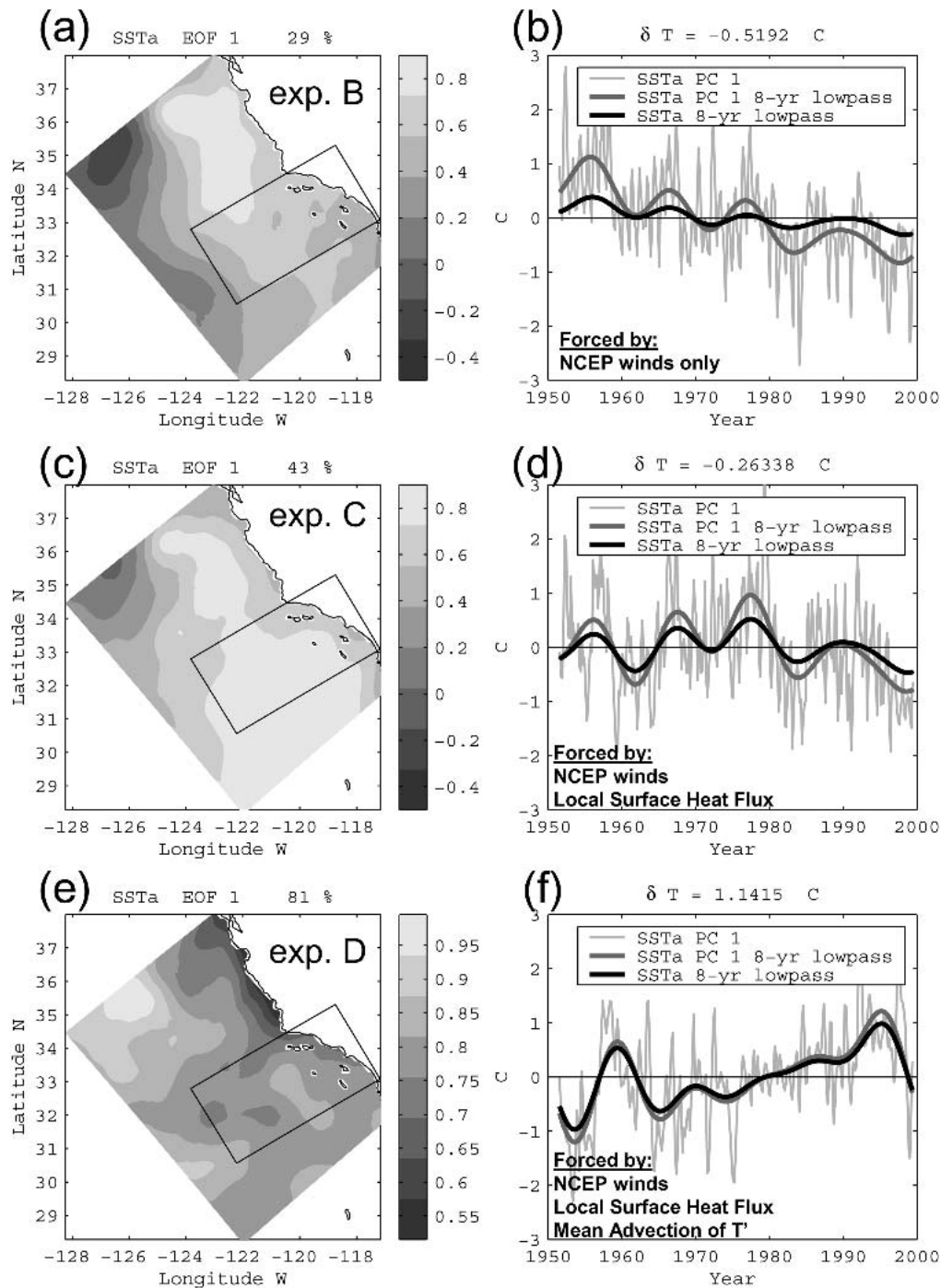


FIG. 14. EOF 1 for SST anomalies for model expts B, C, and D. The seasonal cycle is removed. The black line in each PC 1 panel represents the model domain average SST anomaly. The figure shows the model SST response to the different forcing functions listed in the right panels.

warmer waters offshore. The core of cold waters is slightly detached from the coast and stronger in the north. This detachment is a result of the transport of warmer water from the south by the coastal poleward flow that develops during summer and autumn. The net temperature change over the 50 years estimated by this model run is -0.51°C . This cooling is calculated by fitting a linear trend to the time series of domain-averaged model SST (Fig. 14b). This time series exhibits a weaker trend than PC 1, suggesting that other processes are also important in regulating the SST. However, this model result strongly suggests that changes in the winds and the consequent response of coastal upwelling have a net cooling effect on the SCCS and therefore cannot explain the warming trend.

b. Response to surface heat fluxes

To understand the role of local surface heat fluxes we consider model experiment C. This experiment includes time-dependent net surface heat fluxes from COADS in addition to the NCEP winds. The model SST response is characterized by EOF 1 (Figs. 14c and 14d) explaining 43% of the variance. This first mode is spatially uniform over the model domain with a change of sign in the northwest boundary. The temporal evolution of EOF 1 does not show the strong cooling trend associated with the winds found in experiment B, but is characterized by decadal variations consistent with the changes in the surface heat fluxes (Fig. 2b). This suggests that changes in surface heating, rather than winds, exert a dominant control on SST. However the model response to local surface heat flux forcing is unable to explain the observed warming. A linear fit to the domain average SST for experiment C results in a net cooling of -0.26°C over the last 50 years. One explanation of why the model does not capture the observed warming trend is related to the use of a climatological open boundary.

The nudging to climatological values of temperature at the open boundaries does not allow for propagation of any signal from outside the model domain. This type of condition is useful to assess the role of local forcing versus remote. However, this type of open boundary condition causes model SST anomalies in the interior to be damped to zero and therefore to have a very short persistence. The time scale over which the relaxation is effective is estimated from the model to be roughly 3 yr.

Because the surface heat fluxes are forcing the ocean SST coherently and in phase over a much larger domain than the model (Fig. 2), this relaxation to climatological values at the open boundaries is inadequate for modeling decadal variations. The surface heat fluxes force ocean temperature anomalies also outside the model domain that are then advected into the model domain by the mean ocean currents. This adds persistence to heat-flux-driven changes in SST. We therefore perform a model simulation in which we nudge the open ocean boundaries to track the observed vertical changes in

CalCOFI temperatures (expt D). The model SST response (EOF 1; Figs. 14e,f) now shows the same warming trend as in the CalCOFI observations (a net warming of 1.14°C from 1950 to 1999) and confirms the importance of mean ocean currents in transporting temperature anomalies.

One could argue that the model only captures the trend because it is artificially prescribed by the relaxation at the open boundaries. However, an additional run of the model that only prescribes open boundary temperature and climatological surface heat fluxes in the interior reveals that model temperature visibly lags the observed by several years. EOF 1 for this experiment also gives rise to a strong boundary layer that separates the open-boundary nudged solution with the interior. The unphysical boundary layer disappears if the heat flux forcing is included for the model interior solution. This confirms that the role of the open boundary relaxation and mean currents is to add persistence in the SST anomalies (SSTa) forced by the heat flux. To better clarify the role of the heat flux and the persistence deriving from the large-scale uniform pattern of the heat flux forcing (Fig. 2), we reinterpret the PE model results with a toy model of temperature forced by the observed heat fluxes.

c. Toy model for temperature variations

Let us start by reconsidering experiment C in a simple dynamical framework

$$\frac{\partial \tilde{T}}{\partial t} = \frac{\tilde{Q}}{\rho C_p H} - \gamma \tilde{T},$$

where the tilde indicates the model domain average anomalies, ρ is the mean density, C_p is the heat capacity, $1/\gamma$ is the damping time scale associated with the relaxation at the open boundary, and H is the average depth of the layer over which \tilde{Q} (surface heat flux anomalies) is acting. For decadal variations in \tilde{T} the depth of H is set to 150 m, as estimated from the vertical extension of the warming in the CalCOFI temperature vertical EOF 1 (Fig. 8a).

We can solve this simple model using the time series of net surface heat flux anomalies (Fig. 2b). The characteristic time scale for $1/\gamma$ is set by $L/U \approx 0.8$ yr, where $L \approx 800$ km is the narrowest extent of the box and $U \approx 3$ cm s $^{-1}$ is the strongest mean current. The solution for \tilde{T} obtained by this simple model is compared with the one obtained by the full physics PE model (experiment C) with open boundary nudging to climatology (Fig. 15a). The solution predicted by the simple model is consistent with that of the PE model. However, these two solutions do not compare well to the observed CalCOFI temperatures (Fig. 15a). This suggests that the simple model in this form (which mimics the PE model with boundary nudging to climatology) is inadequate to explain the observed changes.

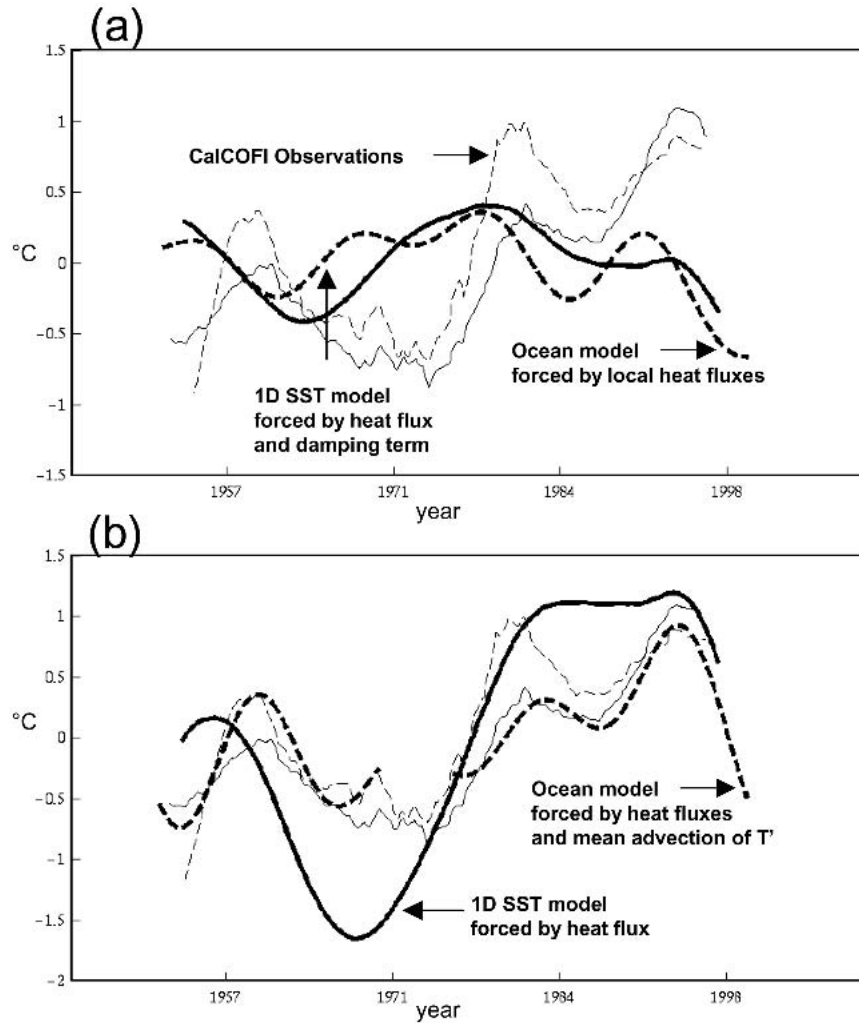


FIG. 15. Time series of SST anomalies for inshore (thin-dashed line) and offshore (thin line) CalCOFI stations. (a) SST anomalies from model expt C (thick-dashed line) and from simple 1D SST model forced by observed heat flux and damping term (thick line). (b) SST anomalies from model expt D (thick-dashed line) and simple 1D SST model forced by observed heat flux but no damping term (thick line).

We now eliminate the nudging of temperature anomalies to zero at the open boundaries, as we did in the full physics model, and allow the persistence of the temperature anomalies. This reflects the idea that the surface heat flux is forcing temperature anomalies over a domain much larger than that of the model. We therefore solve our simple model without the damping term:

$$\frac{\partial \tilde{T}}{\partial t} = \frac{\tilde{Q}}{\rho C_p H}.$$

The new solution for \tilde{T} (Fig. 15b, thick solid line) now tracks the observed interdecadal temperature variations. It captures the proper amplitudes of the cooler period of the 1960s, the transition to warmer conditions during the 1970s, and the commencement of a cooler

climate in the late 1990s. This solution is also consistent with the PE model solution for experiment D, which represents this mechanism by allowing the temperature anomalies to be advected by the mean currents through the open boundaries (Fig. 15b).

These results suggest that changes in ocean temperature along the coast of California occur as a result of spatially coherent changes in surface heat flux forcing acting over the entire eastern North Pacific Ocean. Therefore the observed warming trend between 1950 and 1999 can be largely explained by decadal variations in Q alone. The recent observed cooling after 1998 is consistent with this idea since both the simple and full physics models show the beginning of a negative cooling trend. It is also clear from the discussion of the model results that these temperature variations are

only weakly controlled locally at the coast by changes in upwelling.

9. Changes in property of upwelled water masses

The California Current is characterized by a tongue of fresh and cold water advected from the north (Bograd and Lynn 2003; Bograd et al. 2001; Bray and Greengrove 1993; Chelton et al. 1982; Lynn and Simpson 1987). At the coast in the upwelling boundary layer, the colder surface water advected from the north reinforces the cold water from the upwelling. For coastal surface salinity, in contrast, the advection of the freshwater from the north is opposed by upwelled saltier water. This is reflected in climatological maps of surface temperature and salinity (Levitus et al. 1994; Levitus and Boyer 1994) as a cold, fresh offshore area bounding a colder, saltier inshore area. This implies that the coastal surface salinity budget is to leading order controlled by a local balance of horizontal advection of freshwater from the north and vertical advection of saltier water from the upwelling. Therefore the positive trend in upwelling favorable winds observed in the NCEP and COADS analysis should lead to an increase in salty/cold water masses at the coast and intensify the cross-shore gradients of salinity. Consistent with this idea, model experiment B, which isolates the model response to the NCEP winds forcing, shows a positive trend in coastal surface salinity (Figs. 12c and 12d) and a cooling trend in SST at the coast. (Figs. 14a and 14b).

The analysis of the CalCOFI observations over the last 50 years, however, reveals a transition toward conditions more typical of reduced upwelling, such as a freshening and warming of the surface waters in the coastal upwelling boundary (Fig. 9) and a decline in zooplankton (Roemmich and McGowan 1995). This freshening of surface coastal waters is also reported by two independent analyses of the long-term changes in the CalCOFI dataset by Bograd and Lynn (2003) and McGowan et al. (2003). This freshening is particularly significant in the inshore region. They suggest that the observed increase in stratification associated with the warming trend has reduced the ability of coastal upwelling and vertical mixing to bring saltier subsurface waters to the surface. We test this hypothesis in model experiment D that includes, in addition to the NCEP upwelling-favorable winds, the increase in stratification associated with the warming trend. A comparison of the time series of coastal salinity for this experiment with experiment B (which includes only NCEP winds) confirms that the increased stratification is strong enough to inhibit the otherwise upwelling-favorable conditions (Fig. 16). This result is also evident from the comparison of the model surface salinity EOFs (Figs. 12c,e), discussed in the section on low-frequency salinity variations.

One potential flaw with the model experiment D is

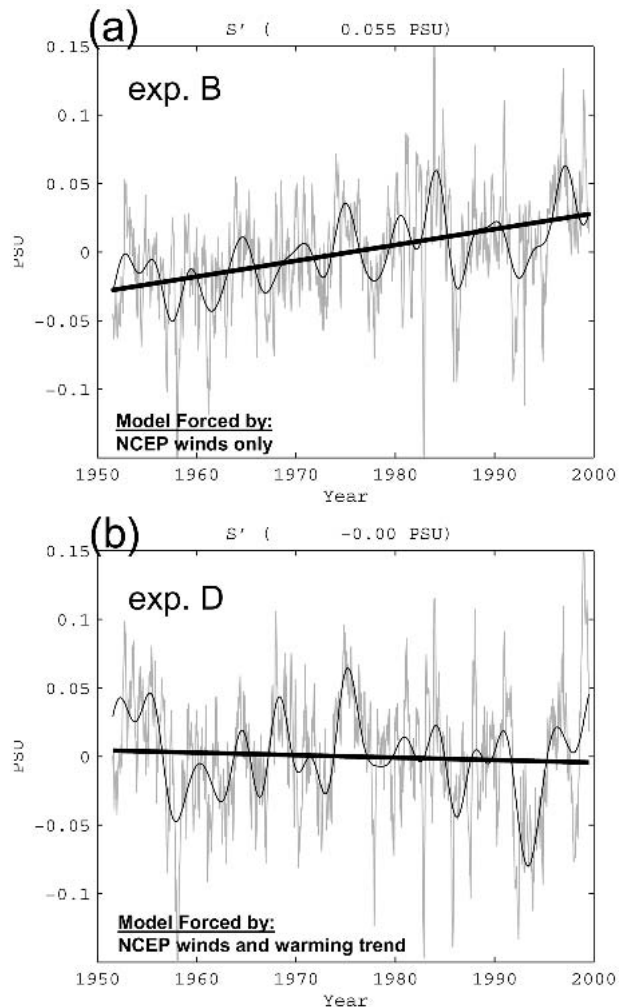


FIG. 16. Time series of model surface salinity anomaly averaged in the alongshore direction following the coast and in the cross-shore direction from 0 to 80 km from the coast. (a) Model expt B and (b) model expt D. Black thick line is 3-yr running average and black thin line is a linear fit to the time series. The figure shows that the increase in stratification associated with the warming trend reduces the efficiency of upwelling to supply saltier water in the coastal boundary.

that adding the observed warm temperature anomalies at the open boundary while leaving salinity at climatological values results in an artificial modification of the T - S relationship. However, in the context of this study we found that the biggest contribution to the warming is the mean advection of temperature anomalies generated by changes in the surface heat fluxes. This exchange of heat occurs through a diabatic process so that to leading order we assume that the warm anomalies have propagated vertically in the water column without affecting open-ocean salinities. To validate this assumption we perform an analysis of the T - S properties of the observed and modeled coastal water masses.

The T - S diagram for the upper-ocean (0–150 m)

coastal water masses (80 km from the coast) for the period before and after the 1970s for the CalCOFI shows the transition toward warmer fresher waters (Fig. 17a). The same diagram for experiment D (Fig. 17c) also shows a transition toward warmer and fresher water masses consistent with the observations. This shift in water masses for experiment D can only be explained by the hypothesis described above (reduction in upwelling efficiency caused by increase stratification) because the introduction of the warm anomalies at the open boundaries while retaining climatological values for salinity would otherwise result in an opposite T - S relationship shift (warmer and saltier). To complete this analysis we also show the results for model experiment B (Fig. 17b). In this experiment the climatological T - S relationship at the boundaries is modified in the surface coastal boundary toward colder and saltier water consistent with the upwelling favorable regime but inconsistent with the observations.

We therefore conclude that stratification exerts a stronger control than the winds on the ability of upwelling to supply salty and cold subsurface water to the surface. The increased stratification over the last 50 years has significantly contributed to the observed freshening of coastal waters in the SCCS. Because the nutrient distributions in the coastal upwelling boundary is similar to salinity, in that they are higher at depth and depleted at the surface, we can deduce that the reduced efficiency of the upwelling has also impacted the coastal nutrient supply and played a role in the observed decline in zooplankton.

10. Changes in eddy variance

Eddies control the cross-shore transport in the SCCS as evidenced by observational studies (Lynn and Simpson 1987; Lynn 1990). The increase in the alongshore winds combined with the deepening trend of isopycnals (and increased stratification) may affect the stability properties, and consequently the eddy statistics of the recirculation region in the SCCS. Since these eddies are likely important for the offshore productivity of the ecosystem we will analyze if significant decadal changes occur in the model hindcasts.

One measure of changes in eddy statistics on decadal time scales is an increase or decrease in velocity anomaly variance. We compare an average cross-shore

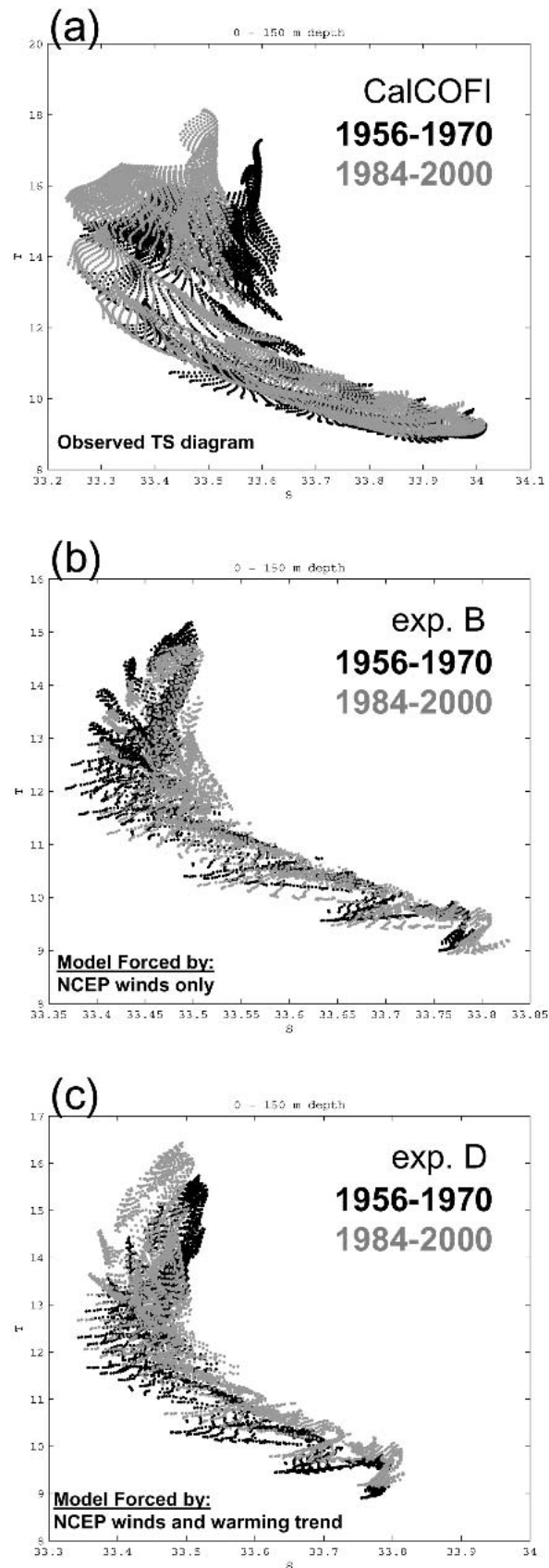


FIG. 17. The T - S diagrams for water masses in the coastal upwelling region (0–100 km from the coast and 0–150-m depth) averaged for the period 1954–70 (black dots) and the period 1984–2000 (gray dots). (a) CalCOFI observations, (b) model expt B, and (c) model expt D. It shows that by including the effect of stratification associated with the warming trend in the model simulation we recover qualitatively the observed T - S relationship in the coastal upwelling region.

section of cross-shore velocity (U) variance for the period E1 (1950s and 1960s) and E2 (1980s and 1990s) from the various PE model experiments. A significant change in variance is found in the offshore waters over the southern California domain south of Point Conception in experiments B and D. These experiments include both isopycnal deepening (associated with the warming) and increasing upwelling winds as forcing functions in the PE model (Fig. 18). The significance was estimated using the F test at the 95% level with 80 degrees of freedom. To compute the degrees of freedom we considered a temporal decorrelation time scale of 3 months. This time scale is a conservative estimate of the typical persistence time of the eddies (1–2 months) in the SCCS (Di Lorenzo et al. 2004).

The increase in variance is also evident in spatial

maps of the differences in eddy kinetic energy for the period E2 minus E1 (Figs. 19b,c). In experiment D, the changes are stronger than in experiment B. This supports the idea that both intensification of the along-shore winds and changes in stratification can produce a change in eddy variance by altering the instability of the currents. We also note that the higher variance is found in the offshore region where the eddies reach their mature stages (Fig. 18a). At the model ocean boundaries the smaller change in variance is associated with the sponge layer close to the boundaries, which damps the activity of the eddies.

These results motivate the need to further investigate the dynamical stability properties of the SCCS on long time scales and their effect on the distribution of nutrients and the ecosystem response.

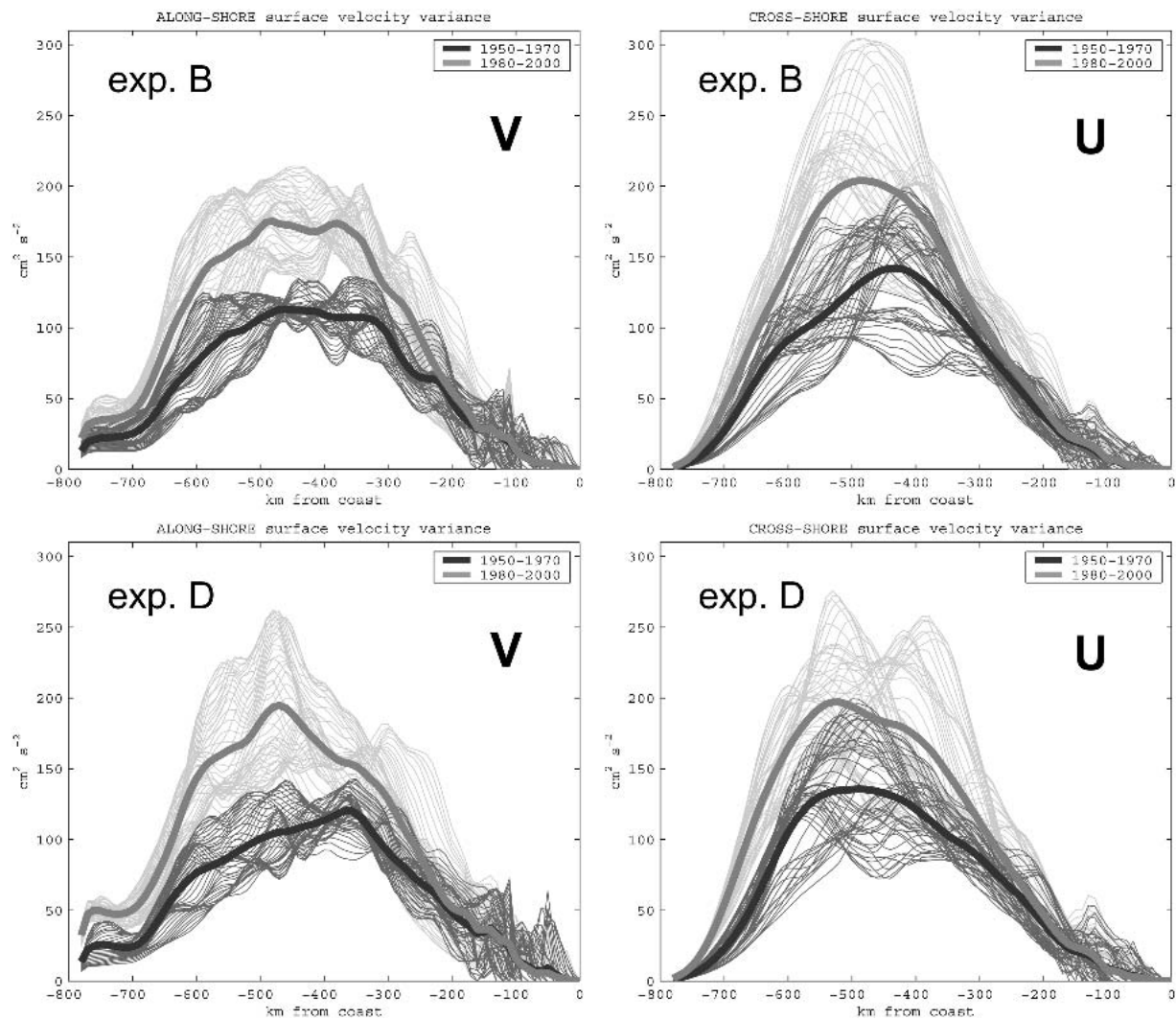


FIG. 18. Average alongshore (V) and cross-shore (U) velocity variance for the periods 1950–70 (dark thick line) and 1980–2000 (gray thick line) as a function of distance from the coast. The average is taken from cross-shore transects between 30° and 34° N. Each member of the average is plotted as a thin line to show the spread. Changes in variance are significant at the 95% level based on an F test with 80 degrees of freedom.

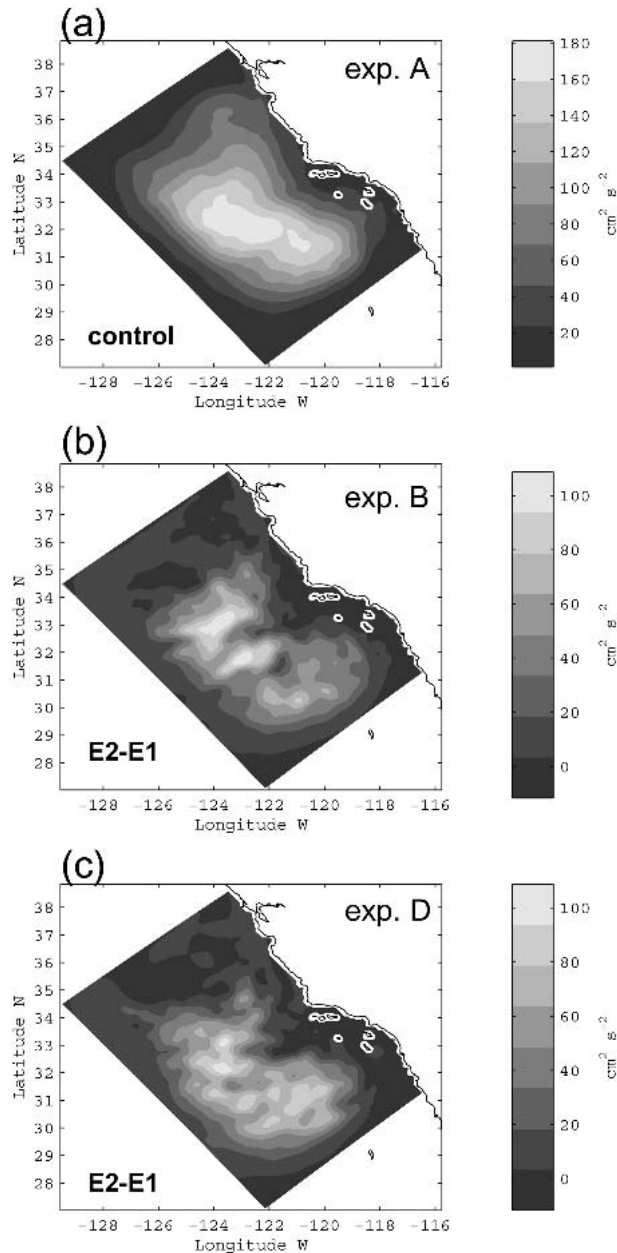


FIG. 19. (a) Model eddy kinetic energy (EKE) for control run (expt A). Difference in EKE for the periods E2–E1 for model (b) expt B and (c) expt D. Period E1 is defined from 1950 to 1970 and period E2 from 1980 to 2000.

11. Summary

The dynamics and thermodynamics controlling the long-term changes of temperature and salinity in the SCCS are reconstructed using a four-dimensional space–time analysis of the CalCOFI 50-yr-long hydrography and a sensitivity analysis of an eddy-permitting primitive equation (PE) ocean model. The PE model experiments are designed to interpret the observations

by supplying insight on the physical processes that cannot be estimated directly from the observations.

A warming trend between 1950 and 1999 of 1.3°C is evident in upper-ocean temperature along the coast of California, together with strong interannual temperature variations. The observed warming trend extends over the top 200 m of the water column and is consistent with large-scale studies of heat content change over the last 50 years (Stephens et al. 2001). The temperature signal is coherent with indices of large-scale climate variability (e.g., PDO) and is uncorrelated with salinity on decadal time scales.

Simple and full physics model experiments reveal that these temperature changes are primarily controlled by changes in net surface heat flux forcing, which acts in phase over the entire northeastern Pacific. Locally in the coastal ocean the persistence of the temperature anomalies is maintained by the southward advection of the mean currents that redistribute the large-scale heat input. These two mechanisms act together to cause a deepening trend in the isopycnals (thermocline depth) and an increase in the stratification over the length of the time series.

It is apparent that the warming trend between 1950 and 1999 is driven in the model by decadal variations, rather than a trend, in Q , suggesting that the observed trend in ocean temperature is part of natural fluctuations of the climate system rather than associated with global warming. Consistent with this interpretation, the observed transition toward cooler temperatures after 1998 is captured by a simple 1D heat flux forced model (Fig. 15b). This does not exclude the possibility that there is also a component of warming trend associated with greenhouse gas increases. However, the temperature variance associated with decadal changes in heat flux is strong enough to inhibit a clear detection of this global warming signal over the length of the CalCOFI record.

Changes in upwelling strength are a weaker contributor to the observed decadal changes of temperature. An SST cooling trend (-0.5°C from 1950 to 1999) occurs in the PE model experiment forced solely by an increase in upwelling-favorable coastal winds over the last decades. This upwelling-forced trend is opposite to the observed warming trend.

An intensification of the mean currents of the SCCS is found in both observations and PE model simulations over the last decades. However, the lack of long-term velocity measurements at other coastal locations does not allow us to establish if these changes are representative of the entire CCS or just locally in the SCCS. In the model this intensification occurs as a response to the increase in upwelling-favorable winds. Model mesoscale eddy variance is found to increase significantly in the recent decades for the experiments that include the increased upwelling-favorable winds and the warming trend. These changes in variance, which likely originate from changes in the dynamical stability property of

the system, cannot be directly estimated from the observations but are potentially an important ingredient toward understanding decadal changes in the ecosystem.

Salinity is characterized by low-frequency variations that do not correlate with indices of large-scale climate variability. These variations are likely associated with the meandering and changes in strength of the CC in the offshore region where the salinity fluctuations have the highest variance. The model hindcasts capture the correct amplitude of the observed signal but are unable to reproduce the correct phasing. A targeted model investigation is being conducted to address this point.

The PE model simulations provide strong evidence that the increase in stratification reduces the vertical transport of nutrient-rich deep water to the ocean surface near the coast (within 50–100 km). The increased stratification counteracts the effects of the increased upwelling favorable winds. This represents a concrete mechanism for explaining the observed decline in zoo-plankton since a lower concentration of nutrients would suppress primary productivity. Further investigation of the impacts of these physical oceanographic changes on the ecosystem of the California Current System is in progress.

Acknowledgments. This study formed a part of the Ph.D. dissertation of EDL at Scripps Institution of Oceanography. Funding was provided by NASA (NAG5-9788), NSF (OCE00-82543), ONR (N00014-99-1-0045), DOE (DE-FG03-01ER63255), and NOAA (NA17RJ1231 through ECPC and CORC). The views expressed herein are those of the author(s) and do not necessarily reflect the views of NOAA or any of its subagencies. Supercomputing resources were provided by the San Diego Supercomputer Center and NASA. We thank our colleagues at Rutgers University (Hernan Arango and Dale Haidvogel) and UCLA (Sasha Shchepetkin and Patrick Marchesiello) for generously allowing use of their computer models and aiding in many aspects of this work. We also thank our CalCOFI colleagues (Teri Chereskin, Ron Lynn, and Tom Hayward) for providing data in accessible form; Dan Cayan for providing the updated surface heat fluxes from his COADS analysis; Peter Niiler, Rick Salmon, and Doug Neilson for many important discussions; and the anonymous reviewer for the comments on the manuscript.

APPENDIX

Error Estimates in Reconstructing the Low-Frequency (Periods > 3 yr) CalCOFI Signal

The CalCOFI dataset is sampled at seasonal resolution (every 3 months). For this reason we choose a 4-month decorrelation time scale in the time optimal interpolation. Although the paper discusses the low-frequency signal (periods > 3 yr), this time interpolation could introduce an aliasing of the high-frequency variance. In this appendix, we try to estimate the un-

certainties associated with the reconstruction of the true low-frequency signal given that we are using an arbitrary 4-month decorrelation time scale in the interpolation.

We use the Scripps Pier SST record for the analysis. This record is located in La Jolla, California, inside the CalCOFI data domain and provides continuous SST data from 1916 to present at monthly resolution (Fig. A1a). From this time series we compute the autocorrelation function that is shown in Fig. A1b. The figure also shows Gaussian autocorrelation functions (of the kind used in the time interpolation) with decorrelation time scales of 2 and 4 months. It is clear that neither Gaussian fits the SST autocorrelation function perfectly. Nonetheless, from this figure we conclude that a 2-month decorrelation time scale would have been a more appropriate choice for the time interpolation of the CalCOFI dataset.

A first look at the spectrum of the Scripps Pier SST record (Fig. A1c) reveals that the time series is not characterized by high-frequency variability but is rather red with enhanced power at the seasonal cycle and at periods beyond 1 yr. This suggests that aliasing of frequencies with periods of less than 4 months (that could occur by applying the 4-month decorrelation time scale in the time interpolation) should not introduce significant errors in our reconstruction of the true low-frequency signal. We quantify the low-frequency error variance due to the aliasing with the following computations.

- 1) We compute the periodogram of the Scripps Pier SSTa (Fig. A1d; the y axis indicates the amount of variance explained by each frequency). The monthly means are removed in computing the anomalies. Figure A1e shows the seasonal cycle from the Scripps Pier SST superimposed on the seasonal cycle from the CalCOFI SST, showing that CalCOFI data accurately capture the seasonal cycle in spite of data gaps.
- 2) We then compute 100 random time series for SSTa that have identical periodograms as the pier SSTa. The random time series were generated by randomizing the phases in the Fourier wave components while preserving the same coefficients.
- 3) We resample each of the randomly generated time series with the same time gap as in CalCOFI (seasonal = every 3 months). We then interpolate each time series at monthly resolution using the 4-month decorrelation time scale and recompute the periodogram. The average periodogram reconstructed from the subsampled/interpolated time series is shown in Fig. A2a.
- 4) We now compute the fraction of the variance that has not been captured by the subsampled/interpolated time series (hereinafter referred to as the “error variance”). For periods greater than 3 yr this amounts to 6%. In the high-frequency bands (below

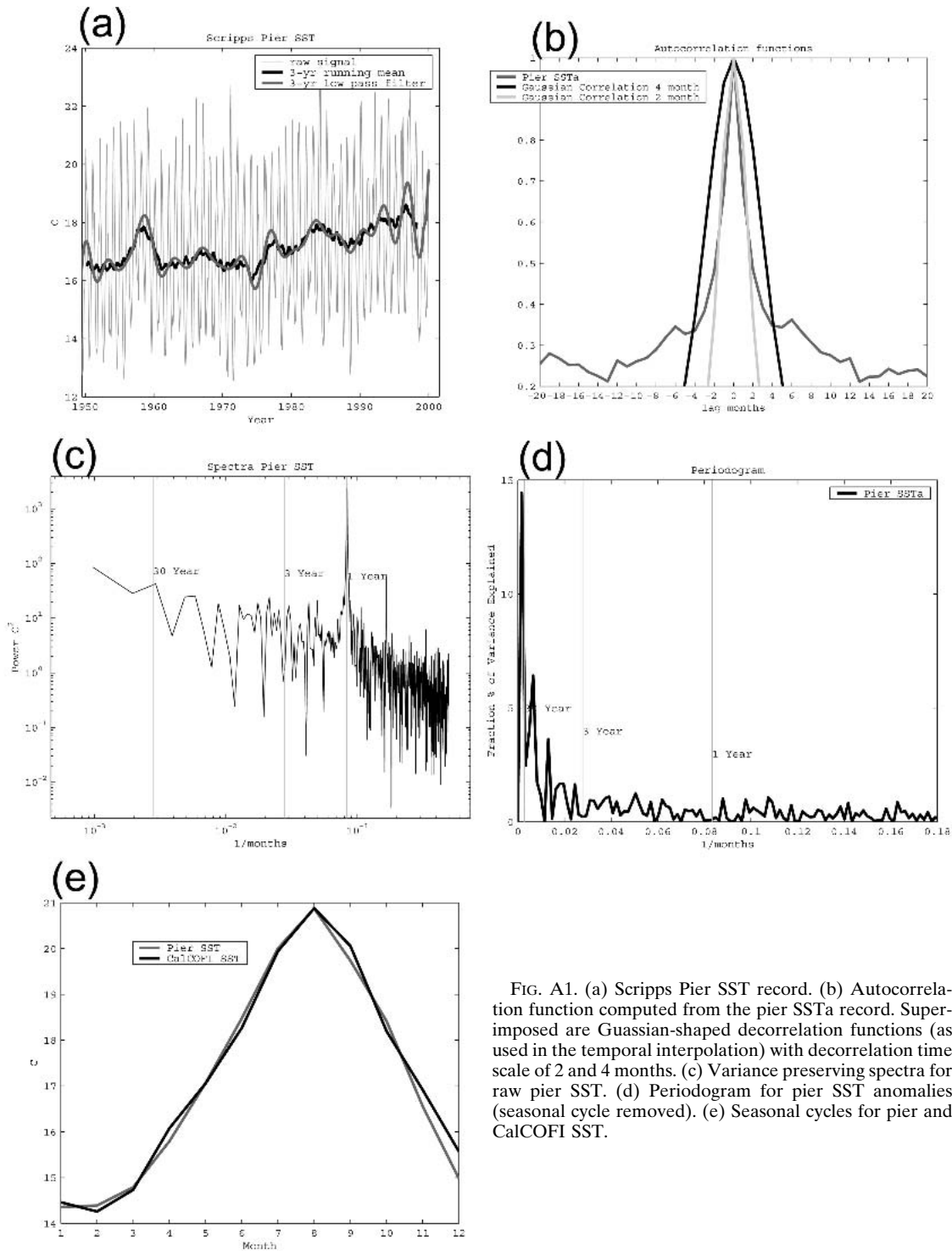


FIG. A1. (a) Scripps Pier SST record. (b) Autocorrelation function computed from the pier SSTa record. Superimposed are Gaussian-shaped decorrelation functions (as used in the temporal interpolation) with decorrelation time scale of 2 and 4 months. (c) Variance preserving spectra for raw pier SST. (d) Periodogram for pier SST anomalies (seasonal cycle removed). (e) Seasonal cycles for pier and CalCOFI SST.

1 yr) the error variance is much worse. However we are not interested in these higher frequencies.

- 5) We perform the same exercise using a time decorrelation of 12 months in the temporal interpolation. The results do not change for the low-frequency

bands, although clearly they do affect the band with periods between 1 and 3 yr (Fig. A2b).

- 6) We then assume that the gaps in the data are more than 3 months and perform the same analysis with data gaps of 4, 5, and 6 months. We find an error

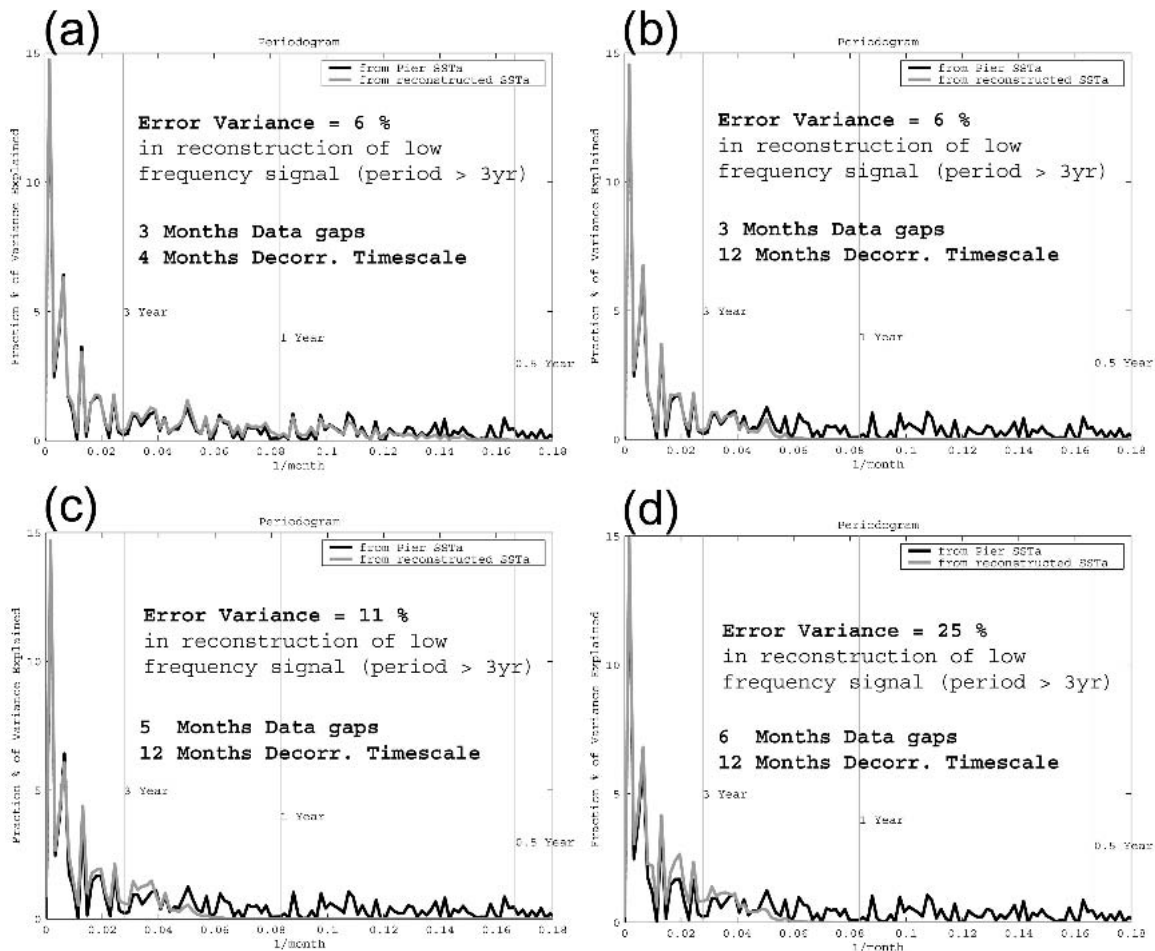


FIG. A2. (a) Pier SST anomalies periodogram and the average periodogram computed from the random subsampled/interpolated time series of SST anomalies. Before computing the average periodogram each of the random time series was subsampled with a time gap of 3 months (as in the CalCOFI data) and interpolated at monthly resolution using the decorrelation time scale of 4 months. In boldface is reported the estimate of the error variance in reconstructing the low-frequency component of the signal (periods > 3 yr). (b) As in (a) but with decorrelation length scale (12 months). (c),(d) Estimates with a bigger temporal gap in the sampling (4 and 6 months, respectively).

variance of 8%, 11%, and 25%, respectively (Figs. A2c,d show the cases with 5- and 6-month data gaps).

The Scripps Pier SST standard deviation is about 1°C , and so a 6% error variance amounts to an uncertainty of $\pm 0.05^{\circ}\text{C}$ in the estimates of the low-frequency signal. Because the coastal SST has shorter temporal decorrelation than deeper temperatures and salinity in this region, we are confident that the error estimates presented above represent an upper limit on the uncertainties. In the analysis of the CalCOFI data we only use the portions of the time series with data points less than 5 months apart. This implies that our uncertainty in reconstructing signals with period above 3 yr is $\leq 11\%$.

REFERENCES

- Bakun, A., 1990: Global climate change and intensification of coastal ocean upwelling. *Science*, **247**, 198–201.
- , and C. S. Nelson, 1991: The seasonal cycle of wind-stress curl in subtropical eastern boundary current regions. *J. Phys. Oceanogr.*, **21**, 1815–1834.
- Bograd, S. J., and R. J. Lynn, 2003: Long-term variability in the Southern California Current System. *Deep-Sea Res.*, **50B**, 2355–2370.
- , T. K. Chereskin, and D. Roemmich, 2001: Transport of mass, heat, salt, and nutrients in the southern California Current System: Annual cycle and interannual variability. *J. Geophys. Res.*, **106B**, 9255–9275.
- Bray, N. A., and C. L. Greengrove, 1993: Circulation over the shelf and slope off northern California. *J. Geophys. Res.*, **98B**, 18 119–18 145.
- Bretherton, F. P., R. E. Davis, and C. B. Fandry, 1976: Technique for objective analysis and design of oceanographic experiments applied to Mode-73. *Deep-Sea Res.*, **23**, 559–582.
- Cayan, D. R., 1992: Latent and sensible heat-flux anomalies over the northern oceans—Driving the sea-surface temperature. *J. Phys. Oceanogr.*, **22**, 859–881.
- Chao, Y., M. Ghil, and J. C. McWilliams, 2000: Pacific interdecadal variability in this century's sea surface temperatures. *Geophys. Res. Lett.*, **27**, 2261–2264.

- Chelton, D. B., P. A. Bernal, and J. A. McGowan, 1982: Large-scale interannual physical and biological interaction in the California Current. *J. Mar. Res.*, **40**, 1095–1125.
- Chereskin, T. K., and M. Trunnell, 1996: Correlation scales, objective mapping, and absolute geostrophic flow in the California Current. *J. Geophys. Res.*, **101**, 22 619–22 629.
- Di Lorenzo, E., 2003: Seasonal dynamics of the surface circulation in the Southern California Current System. *Deep-Sea Res.*, **50B**, 2371–2388.
- , A. J. Miller, D. J. Neilson, B. D. Cornuelle, and J. R. Moisan, 2004: Modeling observed California Current mesoscale eddies and the ecosystem response. *Int. J. Remote Sens.*, **25**, 1307–1312.
- Kalnay, E., and Coauthors, 1996: The NCEP/NCAR 40-Year Reanalysis Project. *Bull. Amer. Meteor. Soc.*, **77**, 437–471.
- Large, W. G., J. C. McWilliams, and S. C. Doney, 1994: Oceanic vertical mixing—A review and a model with a nonlocal boundary-layer parameterization. *Rev. Geophys.*, **32**, 363–403.
- Levitus, S., and T. P. Boyer, 1994: *Temperature*. Vol. 4, *World Ocean Atlas 1994*, NOAA Atlas NESDIS 4, 117 pp.
- , R. Burgett, and T. P. Boyer, 1994: *Salinity*. Vol. 3, *World Ocean Atlas 1994*, NOAA Atlas NESDIS 3, 99 pp.
- Lluch-Cota, D. B., W. S. Wooster, and S. R. Hare, 2001: Sea surface temperature variability in coastal areas of the north-eastern Pacific related to the El Niño–Southern Oscillation and the Pacific decadal oscillation. *Geophys. Res. Lett.*, **28**, 2029–2032.
- Lynn, R. J., 1990: The flow of the undercurrent over the continental borderland off southern California. *J. Geophys. Res.*, **95**, 12 995–13 008.
- , and J. J. Simpson, 1987: The California Current System—The seasonal variability of its physical characteristics. *J. Geophys. Res.*, **92B**, 12 947–12 966.
- Mantua, N. J., S. R. Hare, Y. Zhang, J. M. Wallace, and R. C. Francis, 1997: A Pacific interdecadal climate oscillation with impacts on salmon production. *Bull. Amer. Meteor. Soc.*, **78**, 1069–1079.
- Marchesiello, P., J. C. McWilliams, and A. Shchepetkin, 2001: Open boundary conditions for long-term integration of regional oceanic models. *Ocean Modell.*, **3**, 1–20.
- , —, and —, 2003: Equilibrium structure and dynamics of the California Current System. *J. Phys. Oceanogr.*, **33**, 753–783.
- McGowan, J., S. Bograd, R. J. Lynn, and A. J. Miller, 2003: The biological response to the 1977 regime shift in the California Current. *Deep-Sea Res.*, **50**, 2567–2582.
- Mellor, G. L., T. Ezer, and L. Y. Oey, 1994: The pressure-gradient conundrum of sigma coordinate ocean models. *J. Atmos. Oceanic Technol.*, **11**, 1126–1134.
- Miller, A. J., D. R. Cayan, T. P. Barnett, N. E. Graham, and J. M. Oberhuber, 1994: Interdecadal variability of the Pacific Ocean—Model response to observed heat flux and wind stress anomalies. *Climate Dyn.*, **9**, 287–302.
- NGDC, 1998: Digital relief of the surface of the earth. National Geophysics Data Center Data Announcement 88-MG-02, NOAA, CD-ROM.
- Roemmich, D., 1992: Ocean warming and sea-level rise along the southwest United States coast. *Science*, **257**, 373–375.
- , and J. McGowan, 1995: Climatic warming and the decline of zooplankton in the California Current. *Science*, **267**, 1324–1326.
- Schneider, N., E. Di Lorenzo, and P. Niiler, 2005: Salinity variations in the southern California Current. *J. Phys. Oceanogr.*, in press.
- Schwing, F. B., and R. Mendelssohn, 1997: Increased coastal upwelling in the California Current System. *J. Geophys. Res.*, **102B**, 3421–3438.
- Shchepetkin, A. F., 2003: A method for computing horizontal pressure-gradient force in an oceanic model with a non-aligned vertical coordinate. *J. Geophys. Res.*, **108**, 3090, doi:10.1029/2001JC001047.
- , and J. C. McWilliams, 1998: Quasi-monotone advection schemes based on explicit locally adaptive dissipation. *Mon. Wea. Rev.*, **126**, 1541–1580.
- , and —, 2005: The regional oceanic modeling system (ROMS): A split-explicit, free-surface, topography-following-coordinate oceanic model. *Ocean Modell.*, **9**, 347–404.
- Simpson, J. J., and R. J. Lynn, 1990: A mesoscale eddy dipole in the offshore California Current. *J. Geophys. Res.*, **95B**, 13 009–13 022.
- Snyder, M. A., L. C. Sloan, N. S. Diffenbaugh, and J. L. Bell, 2003: Future climate change and upwelling in the California Current. *Geophys. Res. Lett.*, **30**, doi:10.1029/2003GL017647.
- Song, Y. H., and D. Haidvogel, 1994: A semi-implicit ocean circulation model using a generalized topography-following coordinate system. *J. Comput. Phys.*, **115**, 228–244.
- Stephens, C., S. Levitus, J. Antonov, and T. P. Boyer, 2001: On the Pacific Ocean regime shift. *Geophys. Res. Lett.*, **28**, 3721–3724.
- Winant, C. D., and C. E. Dorman, 1997: Seasonal patterns of surface wind stress and heat flux over the Southern California Bight. *J. Geophys. Res.*, **102B**, 5641–5653.
- Zhang, Y., J. M. Wallace, and D. S. Battisti, 1997: ENSO-like interdecadal variability: 1900–93. *J. Climate*, **10**, 1004–1020.